# Acoustic Signature Measurements and Modelling of sUAS Vehicles

**James H. Stephenson**
Aerospace Engineer, U.S. Army Combat Capabilities Development Command
Aviation & Missile Center, MS 461, Hampton, VA, USA 23681
UNITED STATES AMERICA

James.h.stephenson@nasa.gov

## *ABSTRACT*

*An extensive wind tunnel test campaign has been conducted to investigate the acoustic emissions of small unmanned aerial systems. An L26H propeller was tested with and without two upstream wing configurations to determine the effect inflow disturbance has on acoustic emissions. A range of propeller revolution rates, wind tunnel speeds, and yaw angles were investigated, and a subset of the results are documented here. Also documented is an acoustic detection calculation method that was used to determine the effect inflow disturbance on the propeller system has on acoustic detection of UAS vehicles. The data clearly proves that full vehicle aerodynamics are required to predict acoustic detection metrics for UAS vehicles, as upstream bodies provide a tactically significant increase in acoustic emissions of the vehicle.*

## 1.0 INTRODUCTION

Unmanned aerial systems (UAS) are becoming prevalent within the commercial, private, and government sectors. With the rise in such systems comes the natural concern of defending against these vehicles. Research in UAS acoustics is a nascent field, with many researchers beginning to identify and model the aeroacoustic emissions of these vehicles [1-4]. Much of the research in this field appropriately relies on past work investigating larger systems, such as helicopter and propeller aircraft [5]. However, some of the relevant knowledge documented in the literature is unknown by the counter-UAS community, which results in common pitfalls to modelling and acoustic detection efforts of propeller and rotorcraft vehicles.

The acoustic signature of rotorcraft and propeller vehicles are dominated by the aeroacoustic emissions of the rotating system. The aerodynamic physics of the rotating system are described by the well-known Navier-Stokes equations. Those equations can be rearranged using Lighthill's acoustic analogy into an inhomogenous wave equation. Ffowcs Williams-Hawkings formulated the Navier-Stokes equation for use with rotating bodies using Lighthill's analogy, and their formulation forms the basis of modern rotorcraft acoustics understanding today [6].

The Ffowcs Williams-Hawkings equation is given as,

$$\Box^2 p(\mathbf{x},t) = \overbrace{\frac{\partial}{\partial t}[\rho_\infty v_n \delta(f_{surf})]}^{\text{Monopole}} - \underbrace{\frac{\partial}{\partial x_i}[l_i \delta(f_{surf})]}_{\text{Dipole}} + \overbrace{\frac{\partial^2}{\partial x_i \partial x_j}[T_{ij} H(f_{surf})]}^{\text{Quadrupole}}. \quad (1)$$

Here, $\Box^2$ is the the d'Alambert (wave) operator, with $p$ representing the acoustic pressure signature. $\rho_\infty$ is the density of air, $v_n$ is the local velocity normal to the surface of the rotor blade ($f_{surf}$) and $\delta$ is the Dirac delta function. $T_{ij}$ is the Lighthill stress tensor, $H$ is the Heaviside functional and $l_i$ is the local force acting on the rotor blade in the i'th direction. The right-hand side of the FW-H equation are aerodynamic forcing terms of

the acoustic wave equation represented by the left-hand side. The aerodynamics result in forcing terms that act as monopole, dipole, and quadrupole noise sources.

One example of critical knowledge regards the effect of flow recirculation on acoustic experiments of rotating systems when testing rotating systems within anechoic chambers [7, 8]. It is known that the acoustic emissions of rotating systems are primarily a result of the rotor blades moving through the fluid medium (thickness noise) and imposing a force on the fluid medium (loading noise). As the rotating system generates thrust, this results in the movement of the fluid. In a closed chamber, this downwash recirculates around the chamber and is reingested by the rotating system. Ingestion of the turbulent, recirculated flow imposes a new, unsteady load on the rotor system resulting in a modification to the loading noise emitted by the system. This flow recirculation, which can cause an increase in noise in excess of 20 dB at the blade passage harmonics, is not experienced by a rotor system hovering in free flight, outside of a confined environment.

The impacts of flow recirculation on acoustic emissions of small UAS (sUAS) vehicles can be further generalized. Any event that causes a flow perturbation through the rotor or propeller of the sUAS system will impact the acoustic signature of the vehicle. This includes the addition of upstream bodies on a pusher propeller UAS or even the presence of wind in a realistic environment. The effects of upstream bodies on acoustic emissions, and the resulting changes in acoustic detection of UAS vehicles, will be evaluated below.

## 2.0 UAS DETECTION

The most commonly proliferated source of counter-UAS detection systems in the world is the human. UAS vehicles, sUAS in particular, are hard to see, have small radar cross-sections, small heat signatures, and minimal electromagnetic interference emissions. However, they can be relatively loud and produce acoustic signatures in the most sensitive portion of the human audible range. This makes the human, especially the human ear, an excellent source of detection and localization for UAS vehicles.

The US Government has MIL-STD-1474E which provides “sound pressure level limits and measurement procedures to promote personnel safety, speech intelligibility, and security from acoustic detection and recognition” [9]. The MIL-STD-1474E is applied to “all designed or purchased … equipment that emit acoustic noise or contain sources of noise.” The acoustic detection portion of MIL-STD-1474E is discussed in more detail below and is based off the work contained in Reference [10].

Reference [10] was designed to provide aural non-detectability distances for equipment and facilities that accounts for “geometric spreading, atmospheric absorption, ground effect, atmospheric turbulence, refraction due to wind and temperature gradients, barriers, foliage, threshold of hearing, psychoacoustic factors, and background noise at the listener's location.” The limits developed in the standard are intended to be effective under most conditions, and provide an excellent tool to use for this discussion.

The specific limitations of the aural detection code assume that a normal young adult is listening for the sound signature, that the source and receiver are approximately the same height (1.2m), and that the source is a steady, broadband noise source. This source location and type is not directly applicable to UAS emissions, as UAS are typically flying overhead, tonally dominated, and unsteady in nature. However, it is assumed that these effects are minimal for the purposes of this paper. Further research is necessary to determine if this assumption is valid.

The single most important factor in determining aural detection of any materiel is the background noise at the receiver’s location. Reference [10] provides two sets of detection parameters, based on two distinct background noise profiles. ‘Level 1’ background represents a quiet and rural area, with highways and other major roads at least 4 km away from the receiver. ‘Level 2’ background represents the quietest background

noise levels likely to be encountered, with a highway or major road at least 10 km away from receiver. One third octave band levels of the two background levels can be seen in figure 1-1.

The human aural detection model described in Reference [10] employs the absolute threshold of hearing as prescribed in ISO R-226 (1961). The absolute threshold of hearing represents the lowest sound pressure level of a tone that can be detected by the average human, 50 percent of the time. Further, the model prescribed does not allow for binaural detection to occur, as they assumed that the difference between binaural and monaural listening is insignificant. It is currently unknown what impact the use of a tone-based threshold of hearing has on acoustic detection of a broadband noise source.

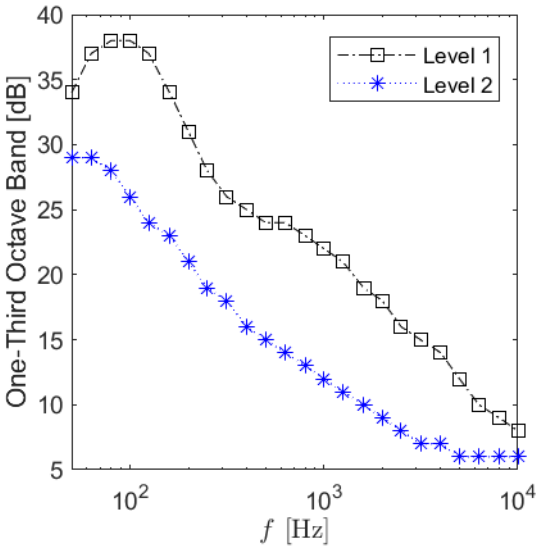


**Figure 1-1: Ambient noise levels as defined by Reference [10].**

The human aural detection model assumes a one-third octave band filter bank. Detection occurs in any one third octave band when a signal (S) to noise (N) ratio (SNR) within any given band is reached. Here, the 'S' is the materiel-produced noise, while 'N' is the background levels previously described.

The human aural detection model takes into account typical signal detection theory parameters. For the purposes of Reference [10], a listener's hit probability was 50%, false alarm rate was 1%, and the listener is 40% as efficient as an ideal listener, with a resulting assumed d' (d-prime) value of 2.32. These parameters are the same used in audiometric threshold tests and are characteristic of highly motivated listeners.

## 2.1 Propagation Implications

Sound pressure levels decrease with spherical spreading in the acoustic far field, which results in a 6 dB reduction per doubling of distance. Further, atmospheric absorption of the acoustic energy will occur, based on the distance travelled, frequency of the signal, and relative humidity of the atmosphere.

Reference [10] uses the 'excess attenuation' model of atmospheric absorption, which accounts for the molecular absorption of energy by Nitrogen atoms at low frequencies as well as the molecular absorption of energy by Oxygen at frequencies above 2 kHz. For the purposes of Reference [10], 15 degrees C and 70% relative humidity are assumed.

Temperature gradients as well as wind velocity and gradients are also known to affect the local convective speed of sound, and therefore acoustic propagation parameters. These effects can result in acoustic shadow

zones as well as ‘hot spots’ of acoustic energy where sound has propagated significantly farther than under uniform conditions. Reference [10] assumes neutral wind and temperature gradients, so that these factors do not unduly influence the results.

The ground is also an acoustically complex reflecting surface, which acts on both amplitude and phase of the incident acoustic wave. In the ideal world, ground reflections can cause perfect cancellation or doubling of the acoustic emission. In reality, it has been shown by References [11-13] that the ground can provide up to 20 dB of attenuation to a 6 dB of enhancement depending on ground impedance parameters, and is heavily dependent on the source and receiver heights above ground level.

For the purposes of Reference [10], the ground was assumed to be uniform and covered in grass, so a ground resistivity of 200 Rayls was used. Foliage and other barriers to sound propagation have also been assumed to be sparse or non-existent, and so are not accounted for in Reference [10]. Further, the source and receiver were assumed to be approximately the same height above ground level (1.2 m), which is not directly applicable for UAS applications.

The ultimate result of the chosen propagation parameters is that detection distances using this model are likely under-predicted for UAS applications. However, they should still provide useful differences for the analysis below.

### 2.2 MIL-STD-1474E Appendix C Use

Finally, MIL-STD-1474E is used to specify the desired acoustic detection distance for a new piece of equipment [9]. As such, it has taken all of the limitations and implications within Reference [10], with some potentially undocumented updates, and produced two look-up tables for acoustic detection. Each background noise level (level 1 and 2) has its own look-up table. In each table the user chooses the preferred detection distance for their new materiel and the table provides the maximum one-third octave band level that should be measured, at a specified distance (2m, 10m, or 30m, depending on detection distance) from the article, to ensure detection does not occur further away than the specified detection distance. This not only provides the government user their choice in detection distance, but also provides the contractor a reasonable and easy way to validate that their materiel meets that detection distance.

## 3.0 EXPERIMENTAL SETUP

An experimental campaign, named the Aerodynamic and Acoustic Rotorprop Test (AART), was undertaken to determine the impacts of a wing positioned upstream of a propeller in a wind tunnel environment [14]. A 4-bladed L26H Sensenich propeller was experimentally tested in the National Full-Scale Aerodynamics Complex (NFAC) under 3 distinct configurations. The propeller was tested (1) without an upstream inflow disturbance device, (2) with a 12 inch chord NACA 0015 “half wing” placed approximately 4 inches in-front of the propeller and stopping prior to the rotor tips and (3) a “full wing” condition where the same wing spans all the way across the propeller. A sketch of each potential configuration can be seen in Figure 3-1.

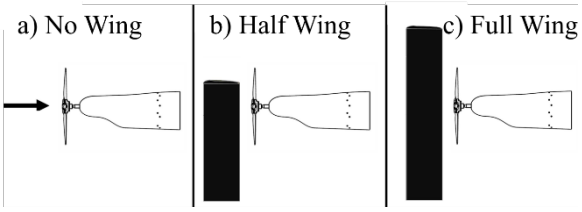


**Figure 3-1: Sketch of AART model wing configurations.**

The NFAC 40- by 80-Foot Wind Tunnel (12.2-m by 24.4-m) is an ideal test facility for aeroacoustic measurements as the walls and floor of the test section are treated with acoustically absorbent material to reduce acoustic reflections, providing an absorptivity of greater than 90% at frequencies above 100 Hz [15]. The AART test stand, is mounted on a three-strut support system at the center of the test-section turntable, seen in Figure 3-2.

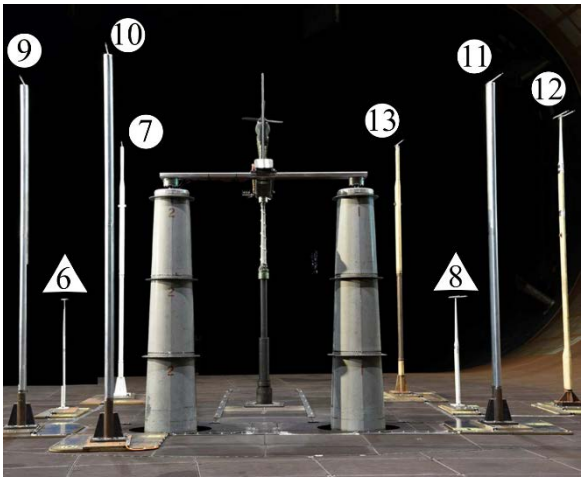


**Figure 3-2: AART with numbered microphone locations in the NFAC 40- by 80-Foot Wind Tunnel test section, view looking downstream.**

Figure 3-2 shows the downstream view of the AART with the full wing configuration in the NFAC 40- by 80-Foot Wind Tunnel. It can be seen that the support hardware for this test are not acoustically treated, so some acoustic reflections off these surfaces are expected.

Acoustic data are acquired by eight microphones that are located around the AART test stand, as seen in Figure 3-2. The microphones are free-field GRAS 40 AC 1/2" microphones coupled with GRAS 26 AJ 1/2 " preamplifiers. Microphones 6 and 8 are placed on 5.625-foot (1.7-m) struts and microphones 7, and 9 through 13, are on 15-foot (4.6-m) struts.

Table 3-1 provides the X, Y, Z, distance (Rd), azimuth angle ($\psi$), and elevation angle ($\theta$) of the microphones, with respect to the propeller center. Here the X-direction is defined as positive in the downstream direction, the Y-direction is positive toward the access door, and the Z-direction is negative down. Figure 3-3 is a top view of microphone locations in the NFAC 40- by 80-Foot Wind Tunnel.

**Table 3-1. Microphone positions for the AART in the NFAC 40- by 80-Foot Wind Tunnel, with respect to center of the propeller. Distance ($R_d$) from hub to microphone as well as azimuth ($\psi$) and elevation ($\theta$) angles are also provided.**

| Mic (#) | X (ft) | Y (ft) | Z (ft) | $R_d$ (ft) | $\Psi$ (deg) | $\Theta$ (deg) |
|---|---|---|---|---|---|---|
| 6 | -0.5 | 10.1 | -9.2 | 13.6 | 93 | -42 |
| 7 | 8.5 | 8.4 | 0.2 | 11.9 | 45 | 1 |
| 8 | -0.6 | -10 | -9.2 | 13.6 | 267 | -43 |
| 9 | -10 | 10.4 | 0.1 | 14.4 | 134 | 0 |

| | | | | | | |
|---|---|---|---|---|---|---|
| 10 | -15.9 | 5.9 | 0.2 | 17 | 160 | 1 |
| 11 | -10 | -10.3 | 0.1 | 14.4 | 226 | 1 |
| 12 | -0.4 | -15.6 | 0.3 | 15.6 | 269 | 1 |
| 13 | 8.5 | -8.4 | 0.1 | 11.9 | 315 | 1 |

(1) Center of coordinate system at rotor hub.

(2) X: Upstream coordinate with negative direction into the wind.

(3) Y: Lateral coordinate with positive toward starboard.

(4) Z: Vertical coordinate with negative downward.

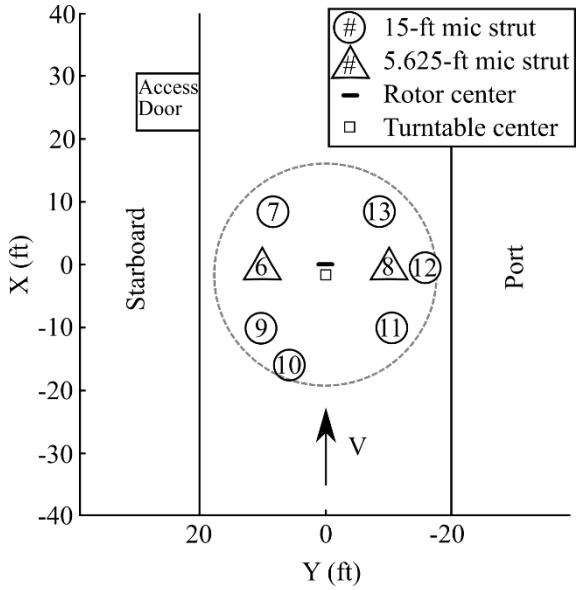


**Figure 3-3: AART with microphone locations in the NFAC 40- by 80-FootWind Tunnel test section, top view.**

All microphone locations are in the acoustic far-field (at least 10 radii from the hub). Microphones 7, and 9 through 13, are at an elevation angle of approximately 0 degrees and have an azimuthal spacing approximately every 45 degrees. This provides a close to uniform azimuthal distribution to validate modelling and simulation tools and is most applicable for aural detection evaluation. Microphones 6 and 8 are in-line with the rotor plane in order to assess symmetry and acquire data that most affect the community during flyover conditions. Results from microphones 6 and 8 will not be evaluated in this paper.

The data recording and encoding equipment consist of: NFAC Data Acquisition system (DAS), NASA supplied Dewetron Data Acquisition System (DDAS), AART RPM encoder, 8 free-field microphones, and

microphone power supply. All microphones were calibrated prior to the test, and calibration was checked in situ using a GRAS Type 42AA pistonphone.

Acoustic data are collected with the NFAC Data Acquisition system (DAS), as well as the NASA supplied Dewetron system (DDAS). The additional data acquisition system from NASA has a higher sampling rate, ideal for acoustic measurements to capture sound at higher resolution (250 kHz per channel). To ensure consistency between the two systems, a start trigger and 1/rev signal were sent from the NFAC DAS to the DDAS. The data acquired from the DDAS were collected at a rate of 250 kHz for 13 seconds to ensure 1,250 revolutions of data were acquired for each test point.

Background noise was acquired for every test point, by collecting acoustic data with the AART stand in the wind tunnel but without the propeller installed. The tunnel fan drive system was turned on to evaluate the noise caused by air flow over the test hardware, as well as from the tunnel drive system itself. Propeller-on testing included multiple sweeps of yaw, pitch, advance ratio, tunnel Mach number (MTun), tip Mach number (MTip), thrust coefficient (CT), and wing configuration.

For the purposes of this paper, we will evaluate two tunnel Mach numbers and two rotor rotation speeds spanning 6000 to 6500 RPM.

## 4.0 DATA PROCESSING AND RESULTS

Calibrated acoustic pressure time histories were harmonically averaged using the 1/rev signal to identify the beginning of each revolution. The 1/rev signal was a “stretched” 1/rev signal, i.e., it has a pulse width longer than the encoder 1/rev. Each revolution is then interpolated to a common sampling rate of approximately 2,048 points per revolution. An ensemble average is then created by averaging across all 1,250 revolutions. This ensemble averaging reduces background noise and suppresses uncorrelated broadband noise from the rotor and wind tunnel system. Figure 4-1 shows the ensemble averaged pressure time history for each of the wing configuration cases at a tunnel Mach number of 0.11 and a rotor RPM of 6000 at 0 degrees yaw.

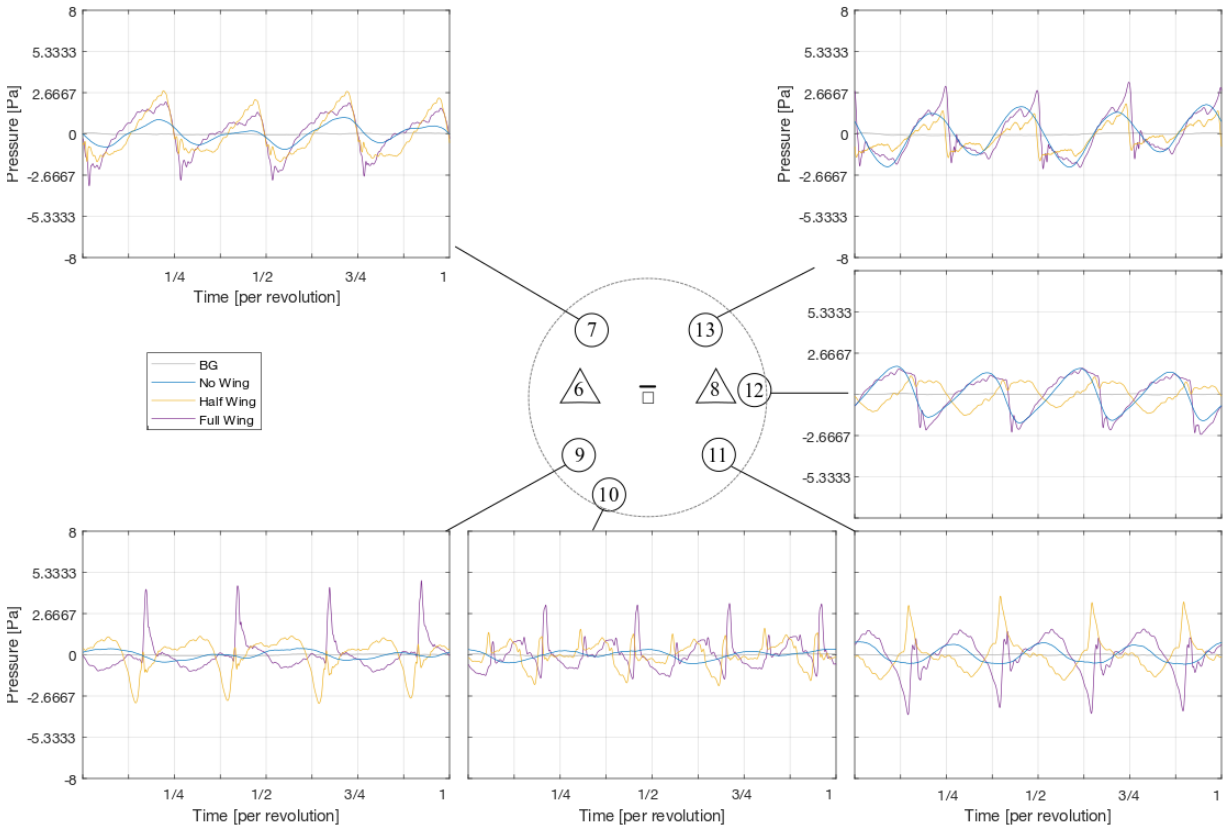


**Figure 4-1: Ensemble averaged pressure time history for each of the wing configuration cases at a tunnel Mach number of 0.11 and a rotor RPM of 6000 at 0 degrees yaw. Ensemble averaged background noise (BG) is also provided to show that it is uncorrelated with rotor RPM.**

The microphones were measured at the same location for every measurement point. However, Reference [9] specifies the required measurement distance and that distance changes based off of the detection distance of the materiel. In order to make use of the model, the ensemble revolution averaged time history for each of the investigated microphones is scaled using spherical spreading to the appropriate distances in the look-up table (2m, 10m, 30m). After scaling to the appropriate distance, the ensemble revolution averaged time history can then be repeated for an arbitrary number of revolutions, and the resulting spectra can be calculated with similar resolution to the original signal. This process produces the average rotor spectra for the tonal components of the signal, and is similar to the process used in Reference [2]. Figure 4-2 shows the resulting narrowband un-scaled spectra of the ensemble averaged time history provided in figure 4-1. Also provided in figure 4-2 is the uncorrelated background noise measurement processed using a half-second increment appropriate for randomly generated noise. This provides some measure of reference for assessing signal to noise ratio of the experimental setup.

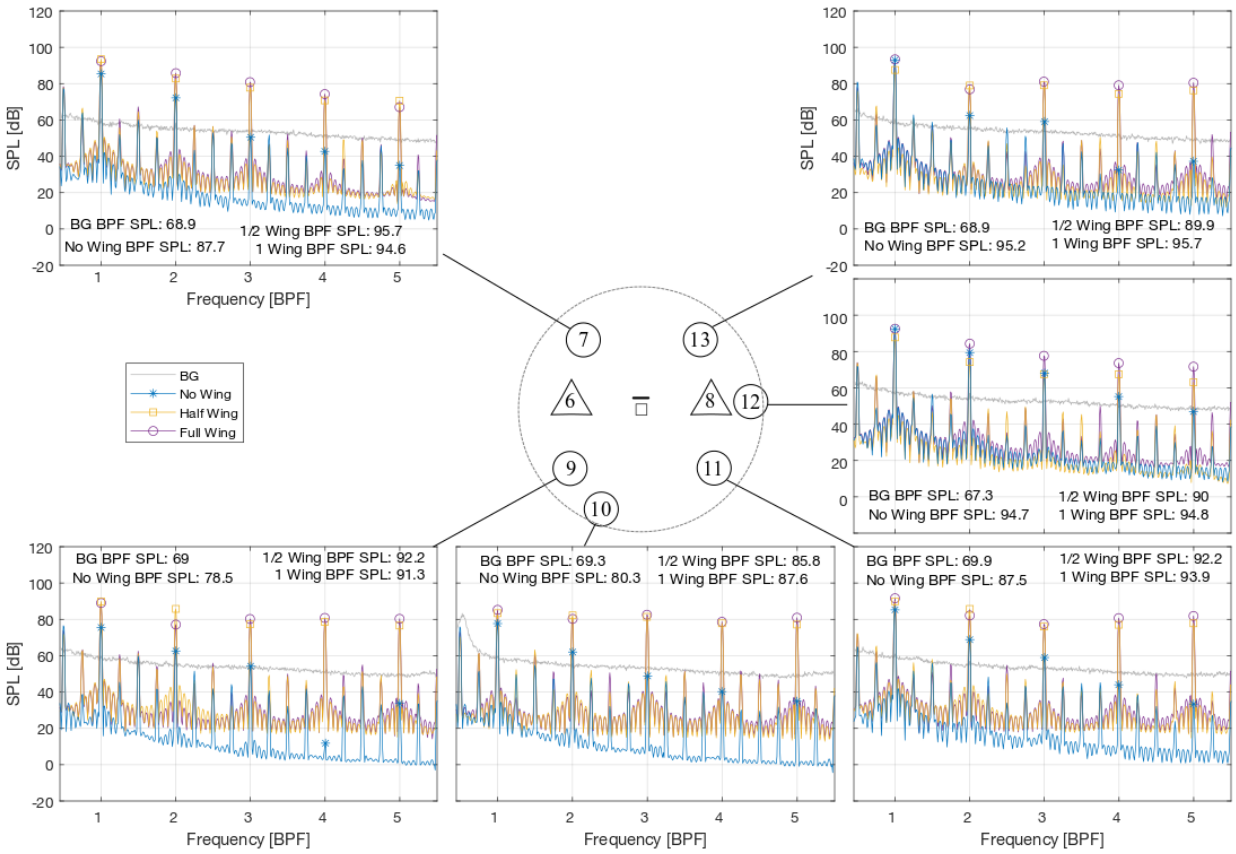


**Figure 4-2: Narrowband spectra of ensemble averaged pressure time history for each of the wing configuration cases at a tunnel Mach number of 0.11 and a rotor RPM of 6000 at 0 degrees yaw. Narrowband background noise (BG) processed in half-second increments is also provided to show uncorrelated background noise levels.**

One-third octave band spectra is then calculated from the scaled narrowband spectra using standard methods and compared to the look-up table provided in Reference [9]. The reported acoustic detection distance for each test point and each direction is reported as the first distance in the lookup table at which the test point was below the allowable threshold for that distance. This process is effectively the reverse method of the intended process, in which we are attempting to determine what the detection distance of the materiel is, instead of determining whether the materiel meets its required threshold. The resulting detection distance for the tunnel Mach number of 0.11 and 6000 RPM condition at 0 degrees yaw is shown in figure 4-3.

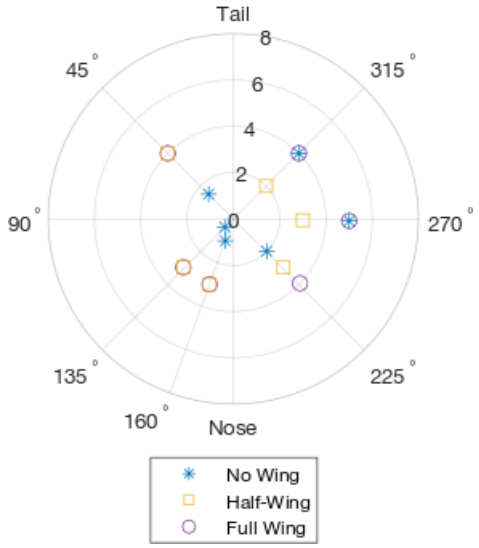


**Figure 4-3: Acoustic detection distance (in thousands of feet) for each of the wing configuration cases at a tunnel Mach number of 0.11, rotor RPM of 6000, 0 degrees yaw, and a level 1 background.**

Now that the process of for evaluating the data for acoustic detection has been established, it is important to look back at the figures and interpret the physics of the situation. Figure 4-1 shows the no wing case in comparison to the half wing and full wing configurations. For the clean, no wing configuration the resulting acoustic emission is as expected for a lightly loaded propeller. Peak acoustic emissions occur in the rotor plane, with minimal emissions forward and slightly larger emissions to the aft of the vehicle. However, adding the half or full wing upstream of the propeller causes a drastic increase in the acoustic emissions forward and aft of the vehicle.

Investigating the effects of the upstream wing on the acoustic emissions, it can be seen in figure 4-1 that the half wing causes a negative pressure pulse while the full wing configuration causes a sharp positive pressure pulse in the forward direction. This pulse is due to the effect of the wing modified inflow on the propeller, resulting in an increase in the loading noise (dipole) term from equation 1. The shape of the noise is a result of whether the inflow disturbance is symmetric across the rotor system or not. The loading noise term is known to propagate predominantly forward and aft of the propeller, and so it can be seen that the values from microphone 12, in the propeller frame, shows only minimal change for these cases compared to the no wing configuration.

The narrowband spectra in figure 4-2 shows some interesting characteristics as well, consistent with the analysis just seen in figure 4-1. It can be seen that the data is harmonically driven at the blade passage frequency, which is 400 Hz for this 4-bladed propeller at 6000 RPM. Subharmonics are seen in the signature which are likely caused by blade manufacturing and wear that was incurred during the wind tunnel testing, as well as vibrations in the test stand. It should be noted that the clean configuration, without the upstream wing, shows a monotonically decreasing sound pressure level at each harmonic which is consistent with theory and past observations. However, the presence of the wing upstream results in spectra that is no longer necessarily monotonically decreasing. For the full wing configuration, microphone 9 shows that the second harmonic is lower than the third through fifth harmonics, while microphone 10 shows that the third harmonic is lower than the fourth or fifth harmonics. Further, an overall escalation in the higher harmonics is experienced, and can be seen in the pressure time series within the sharper pulses previously discussed. Some of the lesser features in the spectra, including the scalloping, are caused by the ensemble averaging and time series repetitions conducted prior to the spectral calculations.

The most interesting results for this condition, however, are found in figure 4-3. In this figure, the aural detection distance for the different wing configurations can be seen, using a level 1 background. Here, the forward radiating direction shows a marked increase in detection distance, from 2000 feet (610 m) or less for the no wing configuration, to up to 4000 (1220 m) feet for the full wing configuration. However, at 270 and 315 degree azimuth a decrease in detection distance can be seen to occur for the half wing configuration. This decrease in detection distance is likely due to a slight destructive interference between the thickness noise (monopole) and loading noise (dipole) terms in equation 1 for this direction and inflow condition. Aeroacoustic modelling of the configuration would have to be conducted in order to verify this assumption. Overall, however, figure 4-3 shows that the presence an upstream body can more than double the aural detection distance for certain directions, especially in the forward facing directions.

It's known that thickness noise scales with propeller RPM, as that increases the normal velocity along the rotor blade. Further, increases in RPM increase the steady loading on the vehicle which will result in increased loading noise. Combined together, this likely results in larger predicted acoustic detection levels for the no wing configuration. In fact, this is what can be seen in figure 4-4, which provides the acoustic detection distance for each wing configuration case at a tunnel Mach number of 0.11 and a rotor RPM of 6500 at 0 degrees yaw. The no wing condition acoustic detection distance has increased compared to the 6000 RPM case shown in figure 4-3. In the plane of the rotor and behind the vehicle, this increase is quite substantial. Further, it can be seen forward of the vehicle the half wing and full wing configurations can result in substantially larger acoustic detection distances due to the inflow disturbance of the wing.

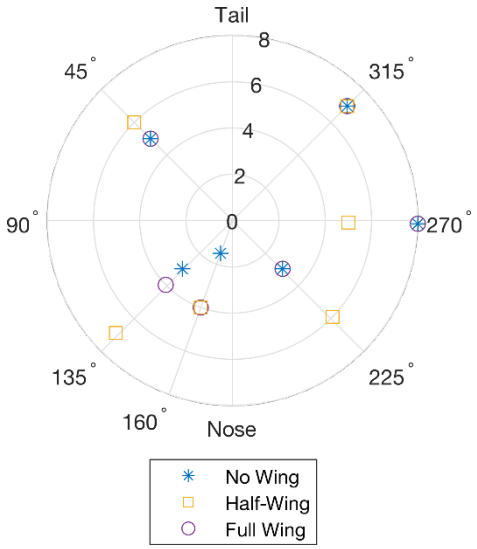


**Figure 4-4: Acoustic detection distance (in thousands of feet) for each of the wing configuration cases at a tunnel Mach number of 0.11, rotor RPM of 6500, 0 degrees yaw, and a level 1 background.**

Higher Mach number cases were also investigated in the course of the wind tunnel test, and a sample of the data from Mach 0.20 is presented in figures 4-5 and 4-6. The increased Mach number of the wind tunnel results

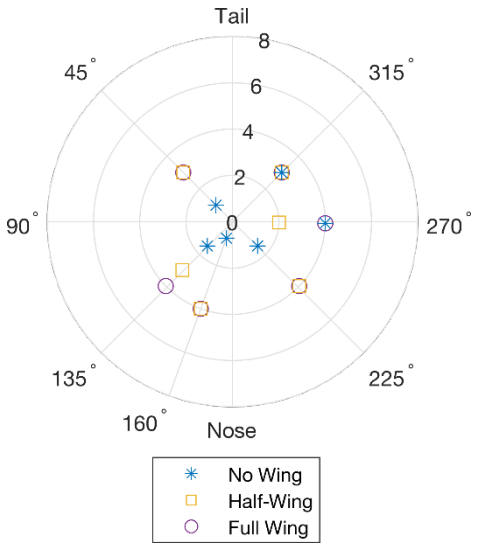


**Figure 4-5: Acoustic detection distance (in thousands of feet) for each of the wing configuration cases at a tunnel Mach number of 0.20, rotor RPM of 6000, 0 degrees yaw, and a level 1 background.**

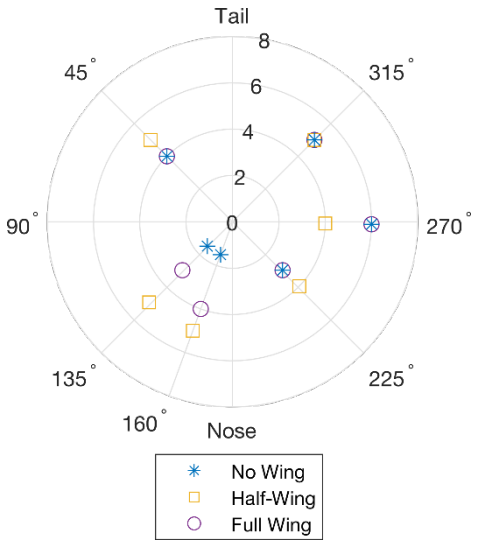


**Figure 4-6: Acoustic detection distance (in thousands of feet) for each of the wing configuration cases at a tunnel Mach number of 0.20, rotor RPM of 6500, 0 degrees yaw, and a level 1 background.**

in a blade loading on the propeller system approximately one-third the level experienced at the same RPM but a Mach number of 0.11. This reduction in the blade loading produces a decreased loading noise and generally results in slightly lower acoustic detection distances for the no wing configurations, as can be seen by comparing figure 4-5 with figure 4-3, or figure 4-6 with figure 4-4. Changes in acoustic detection are also seen with the half wing and full wing configuration cases, where generally speaking the inflow disturbance generated by the upstream body results in increase in the acoustic detection distance of the vehicle compared to the no wing condition.

Figures 4-3 through 4-6 clearly demonstrate that upstream bodies significantly affect the inflow to a

propeller and that inflow change results in meaningful modifications to the resulting acoustic detection distance. This means that modelling the proper aerodynamics of the full vehicle configuration is required for accurately predicting the acoustic detection of UAS vehicles.

## 5.0 CONCLUSIONS

An extensive wind tunnel aerodynamic and acoustic test campaign has been conducted where an L26H propeller was tested in three configurations. The configurations are no upstream wing, a half wing, and a full wing upstream of the propeller. These configurations were used to determine the effect inflow disturbance has on acoustic emissions. A range of propeller revolution rates, wind tunnel speeds, and yaw angles were also investigated, and a subset of the results are documented here.

Also documented is an acoustic detection calculation method that was used to determine the effect inflow disturbance on the propeller system has to acoustic detection of UAS vehicles. The data shows the clear impact rotor inflow disturbances have on the emitted acoustic signature and demonstrates the reason why full vehicle aerodynamic calculations are required to model the acoustic emissions of a UAS.

## REFERENCES

[1] G. Sinibaldi and L. Marino, “Experimental analysis on the noise of propellers for small UAV,” Journal of Applied Acoustics **74**, 79–88 (2013).

[2] N. S. Zawodny, D. D. Boyd, and C. L. Burley, “Acoustic characterization and prediction of representative, small-scale rotary-wing unmanned aircraft system components,” in Proceedings of the 72nd Annual Forum of the American Helicopter Society (2016).

[3] K. Herreman, “Proposed measurement method for UAV sound levels,” in INTER-NOISE and NOISE-CON Congress and Conference Proceedings, NoiseCon16, **8**, Institute of Noise Control Engineering, 615–622 (2016).

[4] C. E. Tinney and J. Sirohi, “Multirotor drone noise at static thrust,” AIAA Journal **56**(7), 2816–2826 (2018).

[5] K. S. Brentner and F. Farassat, “Modeling aerodynamically generated sound of helicopter rotors,” Progress in Aerospace Sciences **39**, 83–120 (2003).

[6] M. J. Lighthill, "On Sound Generated Aerodynamically, I: General Theory." Proceedings of the Royal Society **A221**, 564-587 (1952).

[7] J. H. Stephenson, D. Weitsman, and N. S. Zawodny, "Effects of flow recirculation on unmanned aircraft system (UAS) acoustic measurements in closed anechoic chambers." The Journal of the Acoustical Society of America **145**.3, 1153-1155 (2019).

[8] J. H. Stephenson, D. Weitsman, and N. S. Zawodny, "Mitigating the pitfalls of testing unmanned aerial system vehicles and components in anechoic chambers." The Journal of the Acoustical Society of America **144**.3, 1830 (2018).

[9] “Department of Defense Design Criteria Standard Noise Limits.” U.S. Department of Defense, MIL-STD-1474E, April, 2015.

[10] G. R. Garinther, J. T. Kalb, D. C. Hodge, and G. R. Price, “Proposed Aural Nondetectability limits for

Army Materiel." U.S. Army Human Engineering Laboratory, March, 1985.

[11] M. Delaney, E. Bazley, "A note on the effect of ground absorption in the measurement of aircraft noise." Journal of Sound and Vibration **16**, 315-322 (1971).

[12] C. Chessell, "Propagation of noise along a finite impedance boundary." The Journal of the Acoustical Society of America **62**.4, 825-834 (1977).

[13] G. A. Daigle, J. E. Piercy, T. F. Embleton, "Propagation of noise over short distances above asphalt." The Journal of the Acoustical Society of America **73**.1 (1983).

[14] N. Schatzman, B. Cheung, N. S. Zawody, J. H. Stephenson, D. C. Sargent, "Aeroacoustic Measurements from the Aerodynamic and Acoustic Rotorprop Test (AART) in the NFAC 40- by 80-Foot Wind Tunnel," in Proceedings of the 77th Annual Forum of the Vertical Flight Society (2021).

[15] N. Barbely, C. Kitaplioglu, and W. C. Sim, "Acoustics Reflections of Full-Scale Rotor Noise Measurements in NFAC 40-by 80-Foot Wind Tunnel," American Helicopter Society Specialists' Conference, San Francisco, CA, USA, January 2012.

## AUTHOR/SPEAKER BIOGRAPHY

**James H. Stephenson, Ph.D**

James is an acoustics subject matter expert for the US Army, Combat Capability Development Center Aviation & Missile Center. He specializes in rotorcraft and UAS acoustic measurements from isolated component measurements in anechoic chambers to full-scale flight test measurement campaigns. He serves as the Army Team Lead for the Comprehensive Rotorcraft Acoustic Flight Test Team at NASA LaRC.

# U.S. ARMY COMBAT CAPABILITIES DEVELOPMENT COMMAND – AVIATION & MISSILE CENTER

## Acoustic Signature Measurements and Modelling of sUAS Vehicles

James H. Stephenson, PhD

Aerospace Engineer

DEVCOM AvMC



28 APR 2021

# DEVCOM VISION AND MISSION

## VISION

To be the scientific and technological foundation of the Future Force Modernization Enterprise through world-leading research, development, engineering and analysis.

## MISSION

To provide the research, engineering, and analytical expertise to deliver capabilities that enable the Army to deter and, when necessary, decisively defeat any adversary now and in the future.

**Deliver collaborative and innovative aviation and missile capabilities for responsive and cost-effective research, development and life cycle engineering solutions.**

# BY THE NUMBERS

**11,942** FY20 Strength

**2,982** Civilian

**10** Military

**~8,940** Contractor

## FY20 Funding
**$4.3B**

**4%** Aviation S&T

**5%** Missile S&T

**65%** Army

**26%** other

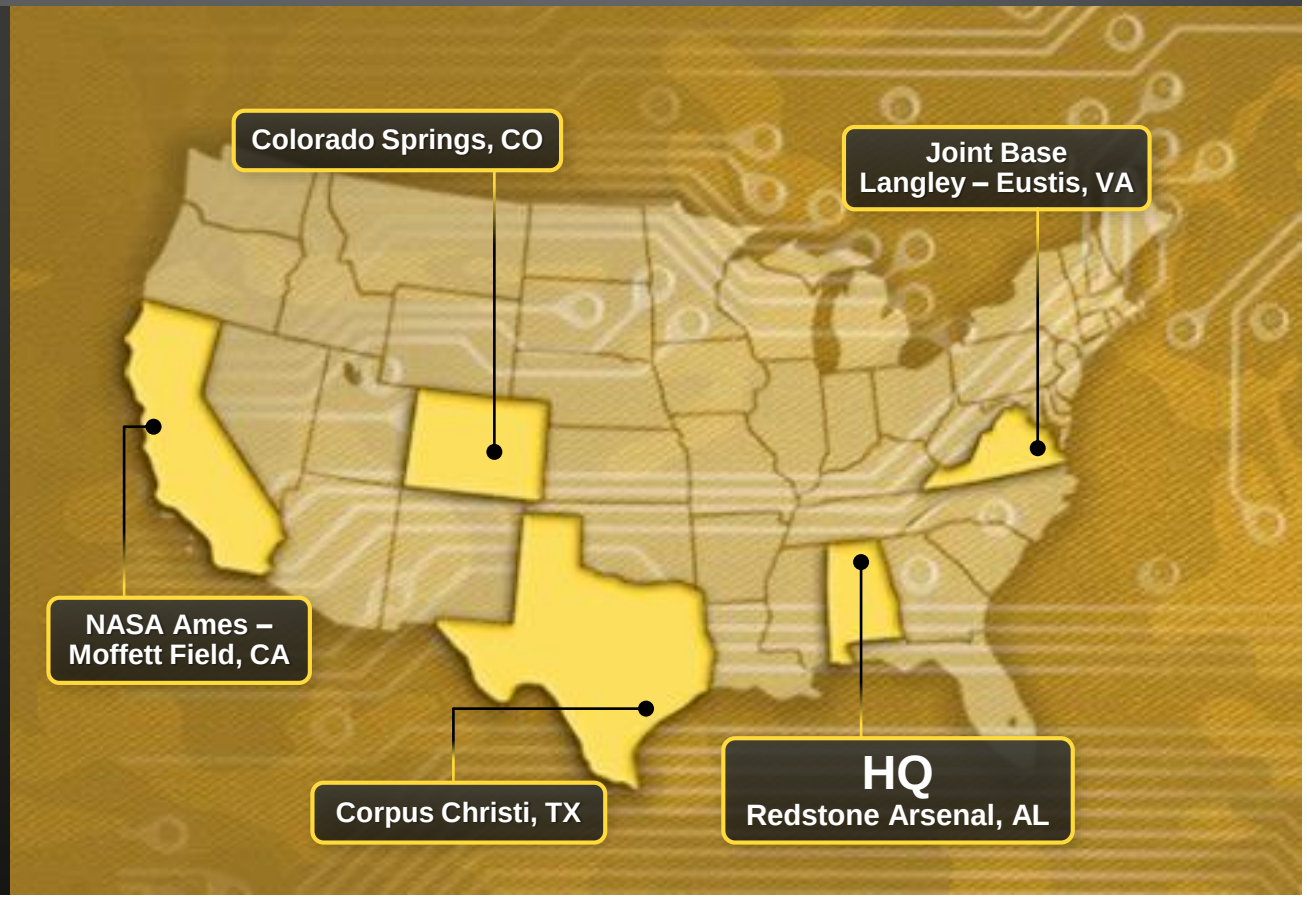


## Core Competencies

***Science and Technology:***

- Materials and Structures
- Guidance, Navigation, Sensors/Seekers
- Propulsion, Explosives, Energetics, Warheads, Fuzing and Actuation
- Air Vehicles Technology
- Aviation Autonomy and Missiles Technology
- Air Defense Sensor Technology

***Capabilities Engineering:***

- Software Engineering
- Weapons Assurance
- Modeling and Simulation
- Configuration Management
- Prototype Design and Development
- Multidiscipline Acquisition and Project Engineering
- Systems Engineering, Integration, and Interoperability
- Airworthiness
- Aviation and Missile Product Performance

## #1: People

People are the Army's greatest strength and its most important weapon system.

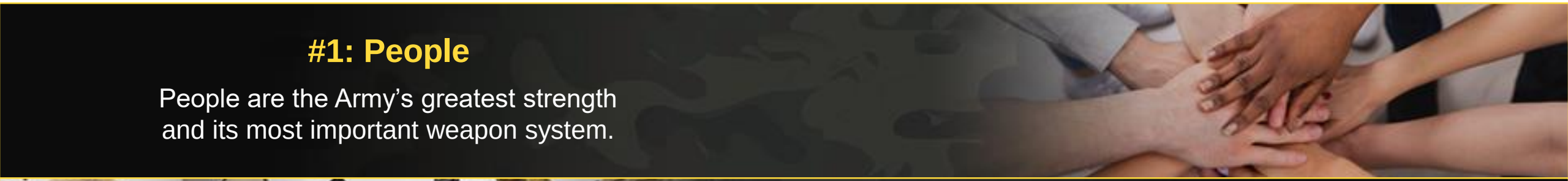

## #2: Readiness

The Army must be ready to defeat any adversary, anywhere, whenever called upon, under any condition.

## #3: Modernization

The Army must modernize to remain lethal and ready to fight tomorrow, against increasingly capable adversaries and near-peer competitors.

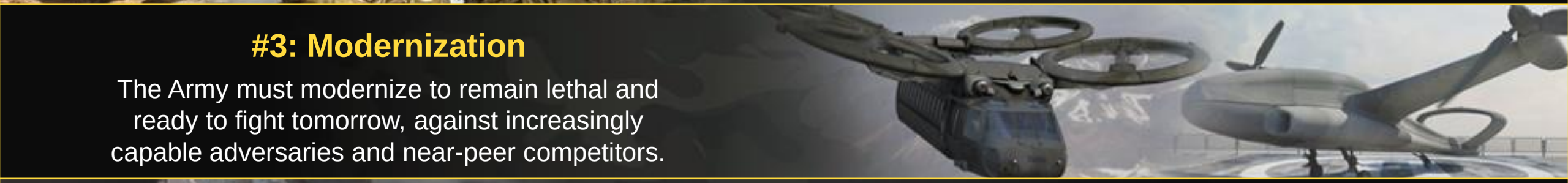

## #4: Reform

The Army will improve the way we do business, including how we implement our top priorities, to make the Army more lethal, capable, and efficient.

LONG RANGE PRECISION FIRES

NEXT GENERATION COMBAT VEHICLE

FUTURE VERTICAL LIFT

ARMY NETWORK

AIR & MISSILE DEFENSE

SOLDIER LETHALITY

## Supporting Army and Joint Readiness now and in the Future MDO Environment

### RESEARCH ISO FUTURE FORCE

Driving the discoveries and innovations which will be critical to realizing new capabilities for the Army of 2030 and beyond.

### ANALYSIS

Conducting objective experimentation and systems analysis to support the equipping and sustaining of our Warfighters.

### ENGINEERING

Providing lifecycle engineering expertise to support fleet development and readiness across warfighting battlefield operating systems.

# ACOUSTIC DETECTION PROBLEM

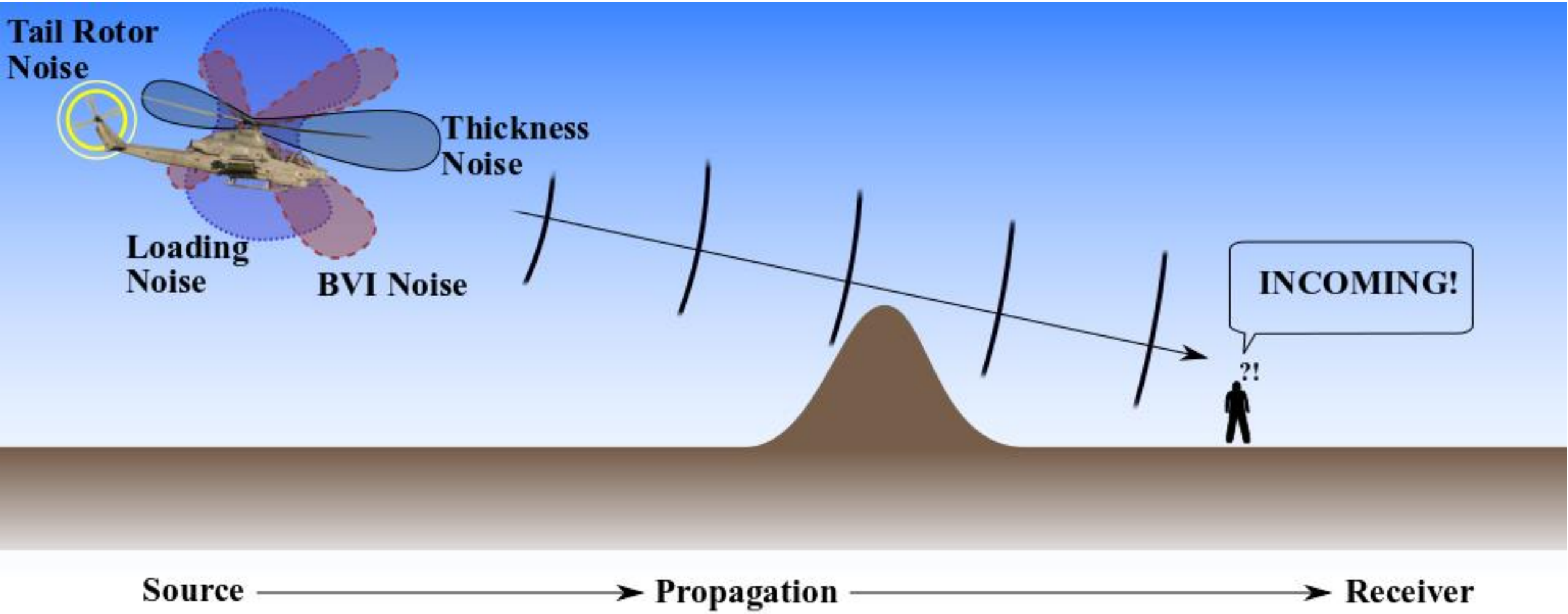

# ROTORCRAFT/UAS SOURCE NOISE

$$p'(\vec{x},t) = \frac{\partial}{\partial t}\iint\left[\frac{\rho_0 v_n}{r|1-M_r|}\right]_\tau dS(\vec{\eta}) - \frac{\partial}{\partial x_i}\iint\left[\frac{p_{ij}n_j}{r|1-M_r|}\right]_\tau dS(\vec{\eta}) + \frac{\partial^2}{\partial x_i \partial x_j}\iiint_V\left[\frac{T_{ij}}{r|1-M_r|}\right]_\tau dV(\vec{\eta})$$

# UAS CONFIGURATIONS

uavos.com

unmanned-ariel.com

glaive.store

wikipedia.org

ecvv.com

challengeraerospace.com


suasnews.com

wikipedia.org

latimes.com

pagerpower.com

time.com

comedronewithme.com

# UAS SOURCE NOISE

## Tractor Configuration

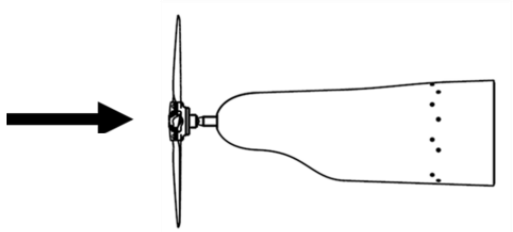

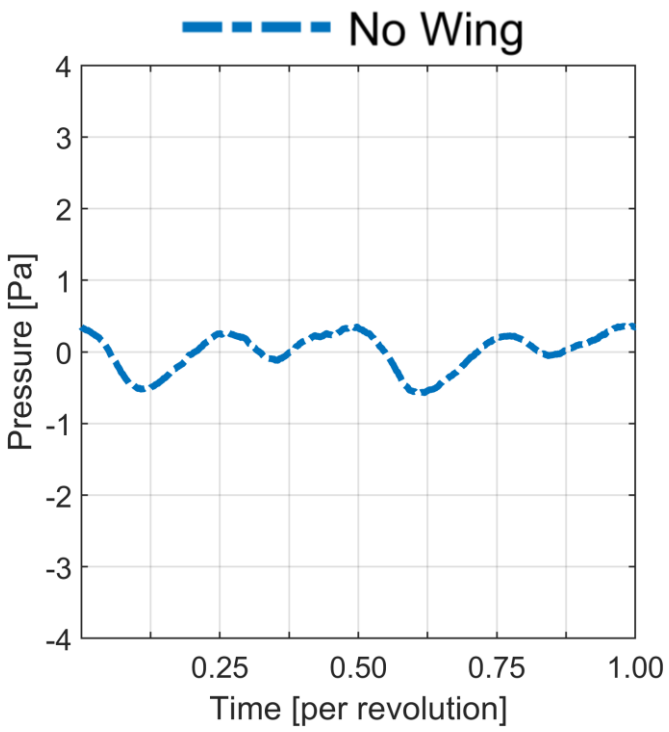


## Pusher Configurations

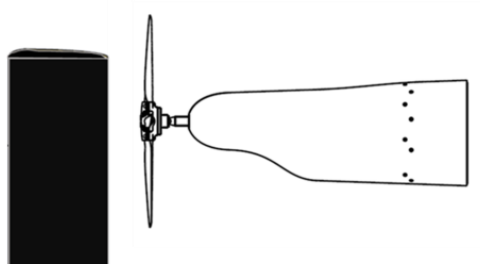

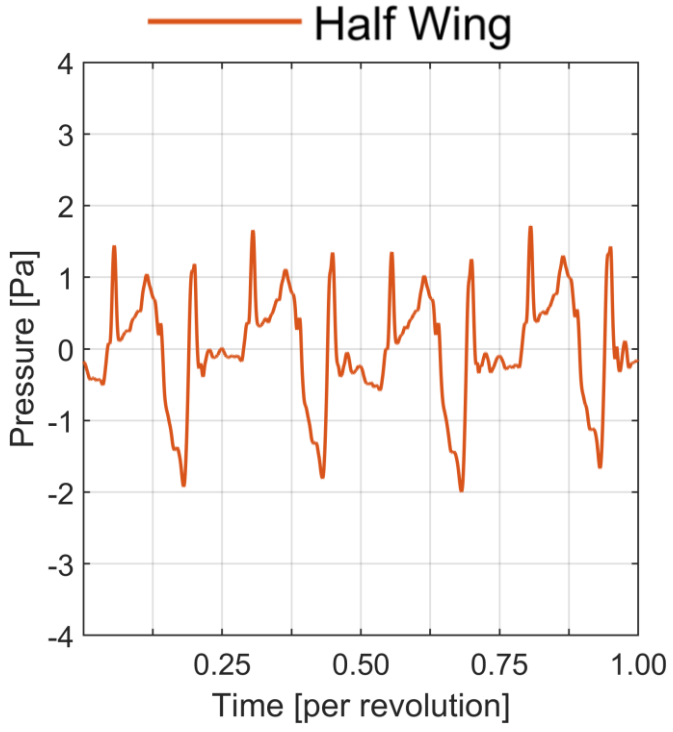


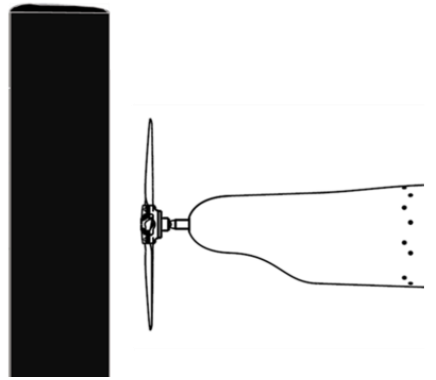

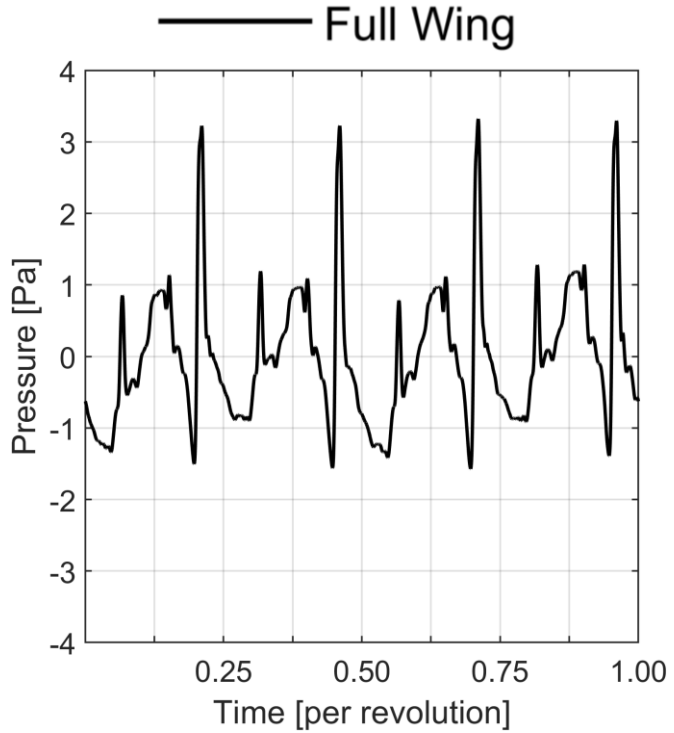

# MIL-STD-1474E: ACOUSTIC DETECTION

- **The MIL-STD-1474E is applied to "all designed or purchased … equipment that emit acoustic noise or contain sources of noise."**

- **Propagation**
  - Geometric Spreading
  - Atmospheric Absorption — 15 degrees C and 70% relative humidity
  - Ground Effect — Uniform and covered in grass, 200 Rayls
  - Atmospheric Turbulence — Negligible
  - Refraction — Neutral wind and temperature gradients
  - Barriers — Non-existent
  - Foliage — Sparse

- **Human Hearing**
  - Threshold of Hearing
  - Psychoacoustic Factors — 50% Pd, False Alarm Rate = 1%, Listener Efficiency = 40% → d' = 2.32

- **Background Noise** — 2 levels; quiet and quieter

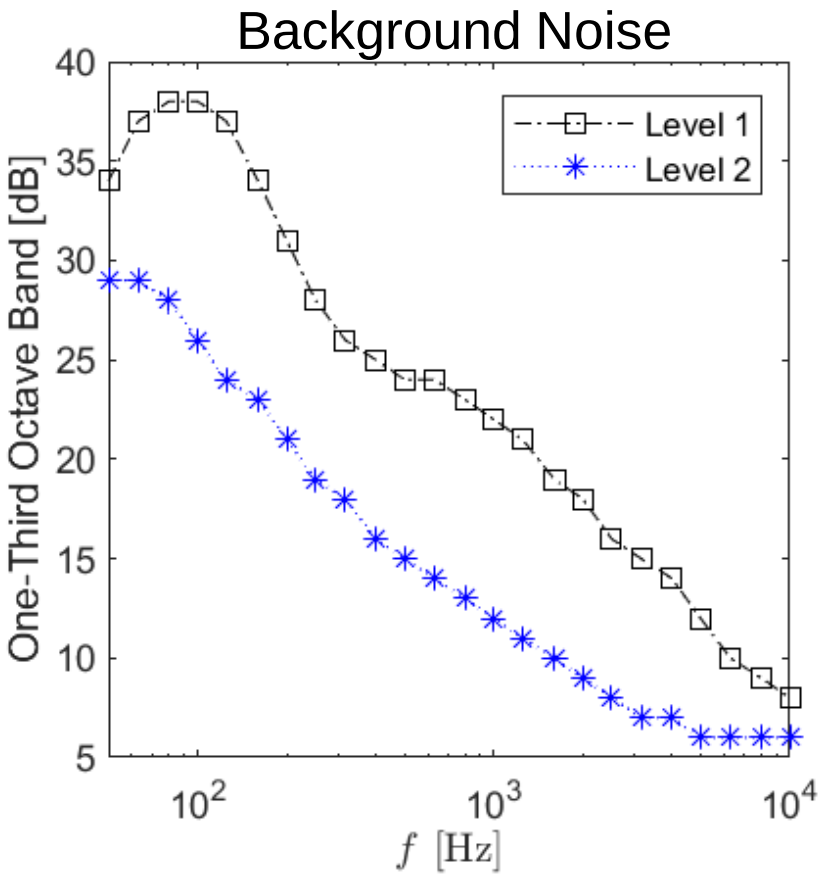

# MIL-STD-1474E: ACOUSTIC DETECTION

| One-Third Octave Band Frequency (Hz) | Non-detectability Distance (meters) | | | | | | | | | | | | | | | | | | | |
|---|---|---|---|---|---|---|---|---|---|---|---|---|---|---|---|---|---|---|---|---|
| | 5 | 10 | 15 | 20 | 25 | 30 | 100 | 200 | 300 | 400 | 500 | 750 | 1,000 | 1,250 | 1,500 | 2,000 | 3,000 | 4,000 | 5,000 | 6,000 |
| 50 | 48 | 53 | 56 | 59 | 61 | 62 | 62 | 68 | 71 | 74 | 66 | 70 | 73 | 75 | 76 | 79 | 84 | 87 | 90 | 92 |
| 63 | 44 | 50 | 53 | 56 | 58 | 59 | 59 | 65 | 69 | 71 | 64 | 68 | 71 | 73 | 75 | 78 | 83 | 87 | 91 | 94 |
| 80 | 44 | 49 | 53 | 55 | 57 | 58 | 60 | 66 | 69 | 72 | 65 | 69 | 72 | 75 | 77 | 81 | 87 | 93 | 97 | 101 |
| 100 | 41 | 46 | 50 | 52 | 54 | 56 | 59 | 65 | 69 | 72 | 65 | 70 | 73 | 77 | 79 | 84 | 92 | 99 | 104 | 107 |
| 125 | 37 | 41 | 45 | 47 | 49 | 51 | 58 | 64 | 69 | 72 | 65 | 71 | 76 | 80 | 83 | 89 | 98 | 102 | 105 | 106 |
| 160 | 36 | 39 | 42 | 44 | 46 | 48 | 55 | 63 | 68 | 72 | 66 | 73 | 79 | 84 | 89 | 93 | 97 | 99 | 101 | 102 |
| 200 | 41 | 42 | 45 | 47 | 49 | 51 | 52 | 61 | 67 | 72 | 68 | 78 | 82 | 85 | 87 | 89 | 92 | 94 | 96 | 98 |
| 250 | 47 | 44 | 47 | 49 | 51 | 53 | 50 | 61 | 69 | 76 | 71 | 76 | 79 | 80 | 82 | 83 | 86 | 89 | 91 | 93 |
| 315 | 44 | 46 | 47 | 50 | 52 | 54 | 50 | 63 | 71 | 75 | 68 | 71 | 73 | 74 | 75 | 77 | 81 | 83 | 86 | 88 |
| 400 | 29 | 43 | 43 | 45 | 48 | 50 | 51 | 62 | 66 | 68 | 62 | 64 | 66 | 67 | 69 | 71 | 75 | 78 | 81 | 84 |
| 500 | 26 | 42 | 47 | 49 | 51 | 54 | 54 | 62 | 64 | 66 | 55 | 58 | 60 | 61 | 63 | 65 | 70 | 73 | 77 | 80 |
| 630 | 27 | 37 | 45 | 49 | 52 | 54 | 55 | 63 | 67 | 68 | 53 | 56 | 58 | 60 | 61 | 64 | 69 | 74 | 78 | 82 |
| 800 | 30 | 31 | 37 | 41 | 44 | 47 | 54 | 63 | 66 | 68 | 54 | 57 | 59 | 61 | 63 | 66 | 72 | 77 | 82 | 87 |
| 1,000 | 25 | 29 | 33 | 37 | 40 | 42 | 50 | 59 | 63 | 65 | 54 | 57 | 60 | 62 | 64 | 68 | 74 | 80 | 86 | 91 |
| 1,250 | 23 | 31 | 32 | 34 | 37 | 39 | 42 | 52 | 57 | 59 | 54 | 57 | 60 | 62 | 65 | 69 | 76 | 83 | 90 | 96 |
| 1,600 | 22 | 31 | 32 | 32 | 33 | 35 | 36 | 46 | 51 | 54 | 52 | 56 | 59 | 62 | 64 | 69 | 78 | 87 | 95 | NAN |
| 2,000 | 21 | 25 | 35 | 32 | 31 | 32 | 36 | 47 | 52 | 55 | 50 | 54 | 58 | 62 | 65 | 71 | 82 | 93 | NAN | NAN |
| 2,500 | 18 | 26 | 26 | 36 | 32 | 31 | 28 | 39 | 45 | 48 | 46 | 52 | 56 | 60 | 64 | 72 | 86 | NAN | NAN | NAN |
| 3,150 | 16 | 21 | 24 | 27 | 36 | 34 | 29 | 40 | 46 | 50 | 41 | 47 | 53 | 59 | 64 | 74 | 94 | NAN | NAN | NAN |
| 4,000 | 15 | 21 | 25 | 25 | 27 | 34 | 25 | 37 | 44 | 49 | 40 | 49 | 57 | 64 | 72 | 86 | NAN | NAN | NAN | NAN |
| 5,000 | 12 | 18 | 22 | 27 | 24 | 25 | 23 | 35 | 43 | 50 | 48 | 60 | 71 | 82 | 92 | NAN | NAN | NAN | NAN | NAN |
| 6,300 | 15 | 20 | 23 | 25 | 31 | 30 | 27 | 40 | 50 | 58 | 56 | 73 | 89 | NAN | NAN | NAN | NAN | NAN | NAN | NAN |
| 8,000 | 23 | 30 | 33 | 35 | 37 | 39 | 40 | 54 | 67 | 78 | 79 | NAN | NAN | NAN | NAN | NAN | NAN | NAN | NAN | NAN |
| 10,000 | 25 | 31 | 35 | 37 | 39 | 42 | 47 | 64 | 81 | 96 | NAN | NAN | NAN | NAN | NAN | NAN | NAN | NAN | NAN | NAN |
| | 2 | 2 | 2 | 2 | 2 | 2 | 10 | 10 | 10 | 10 | 30 | 30 | 30 | 30 | 30 | 30 | 30 | 30 | 30 | 30 |
| | Measurement Distance (meters) | | | | | | | | | | | | | | | | | | | |

Steps for Use:

1) Pick a detection distance you desire (ex: 500m).

2) Find out how far away you need to measure acoustic emissions (ex: 30m)

3) Be under the spectra **listed (in dB).**

# EXPERIMENTAL SETUP

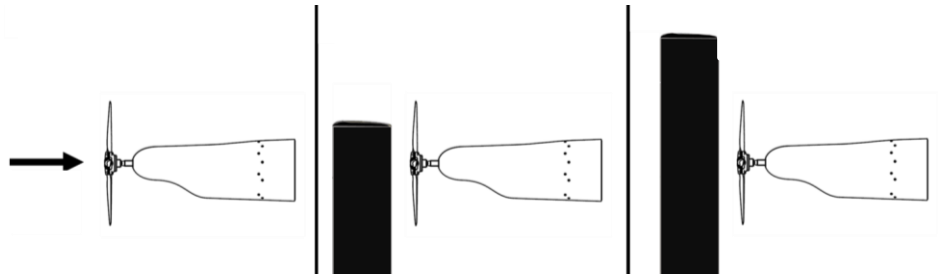

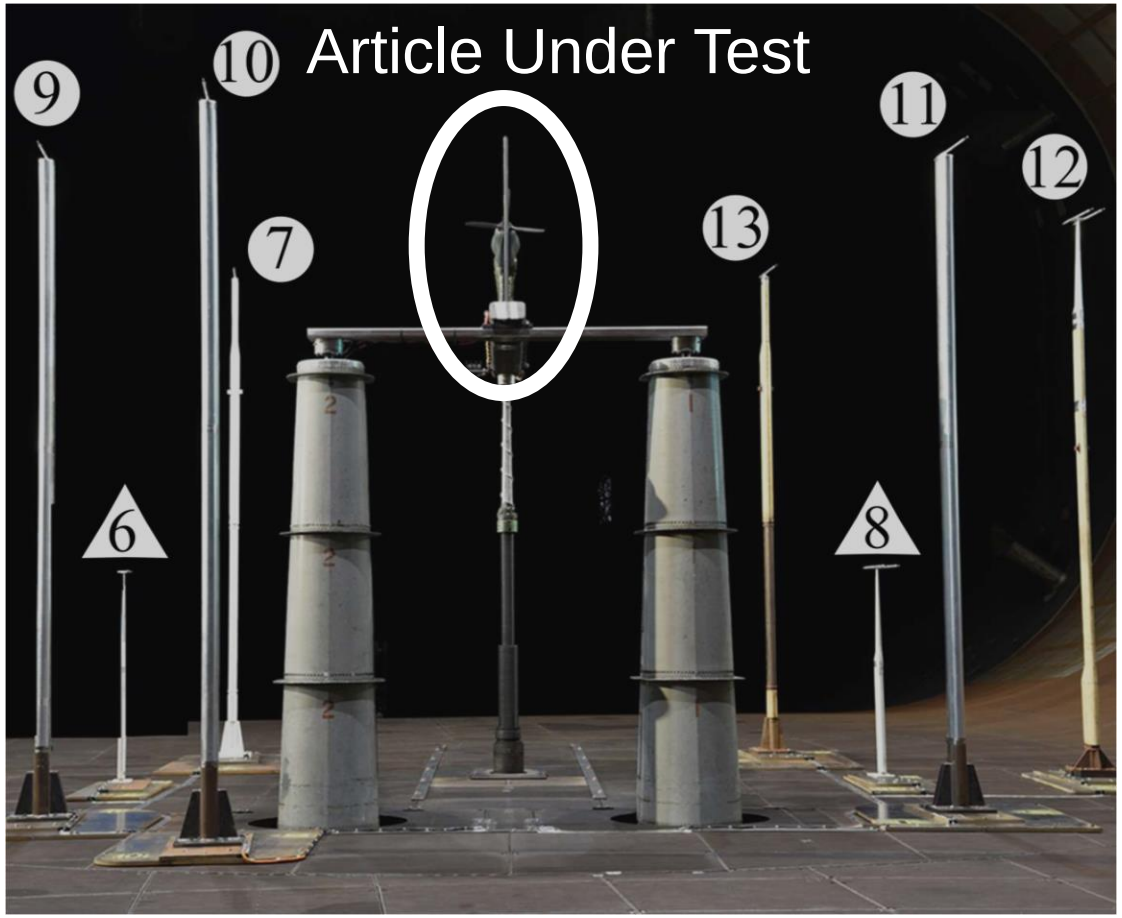


4-Bladed L26H Propeller

NACA 0015 Wing

# EXPERIMENTAL SETUP

## Front View

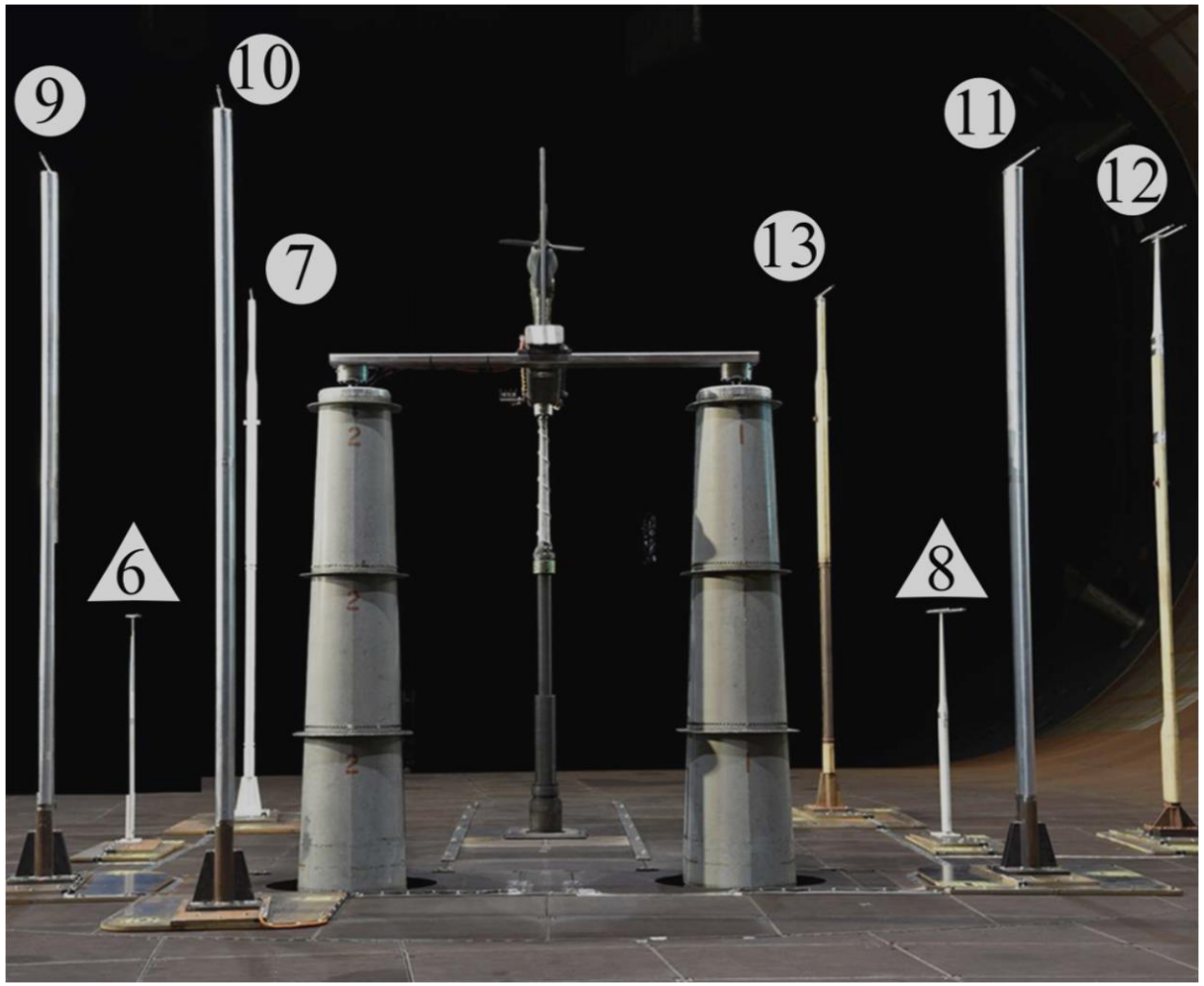


## Top View

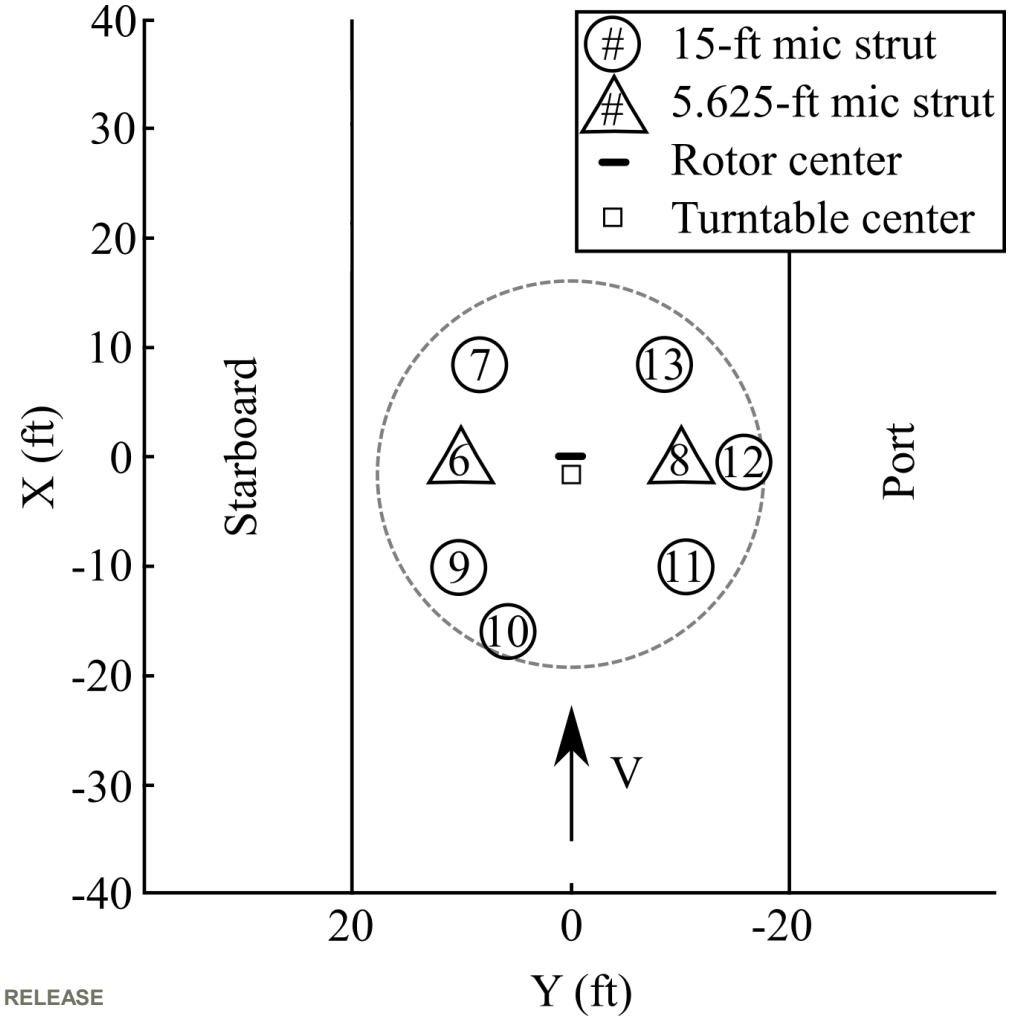

# EXPERIMENTAL DATA

## CONDITION

$M_{TUN}$ = 0.204 (70 m/s)

RPM = 6300

Yaw = 0°

Ensemble averaged pressure

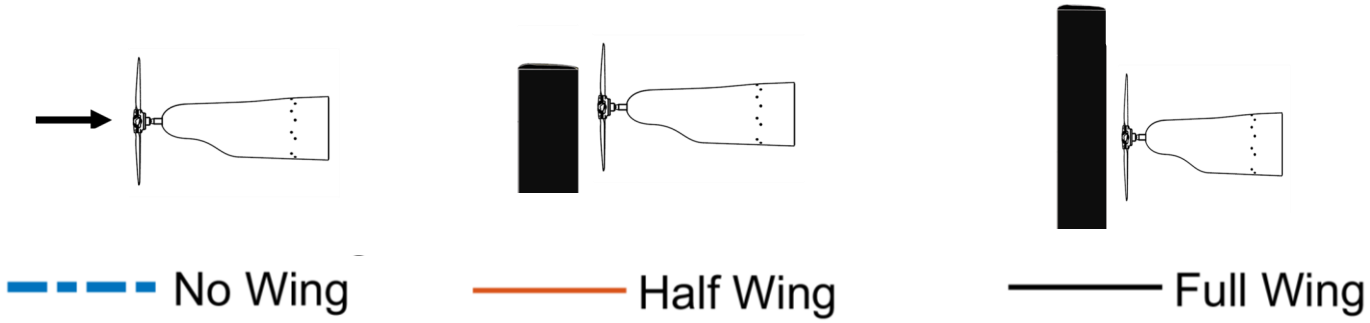


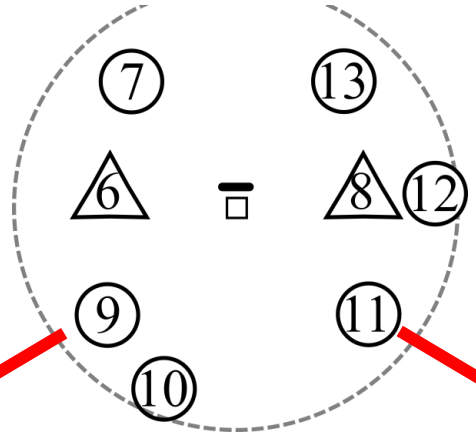


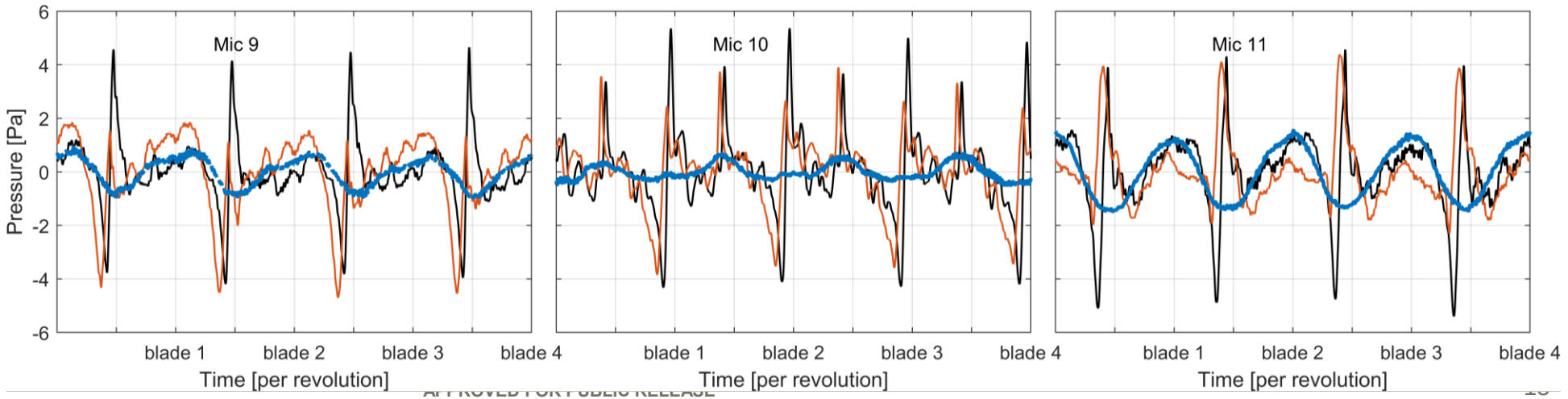

# DATA ANALYSIS

**Fixed Distance Measurements**

↓

**Spherically Spread to Required Measurement Distance**

↓

**Calculate One-Third Octave Spectra**

↓

**Compare to MIL-STD-1474E Table**

↓

**Detection Distance**

# DATA ANALYSIS

## CONDITION

$M_{TUN}$ = 0.204 (70 m/s)

RPM = 6300

Yaw = 0°

Case: Full Wing

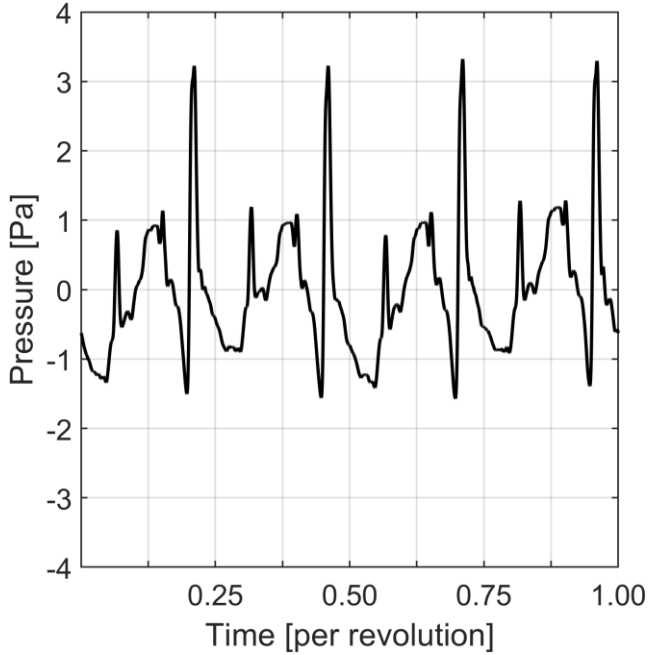


Third Octave Band Spread to Required Distances

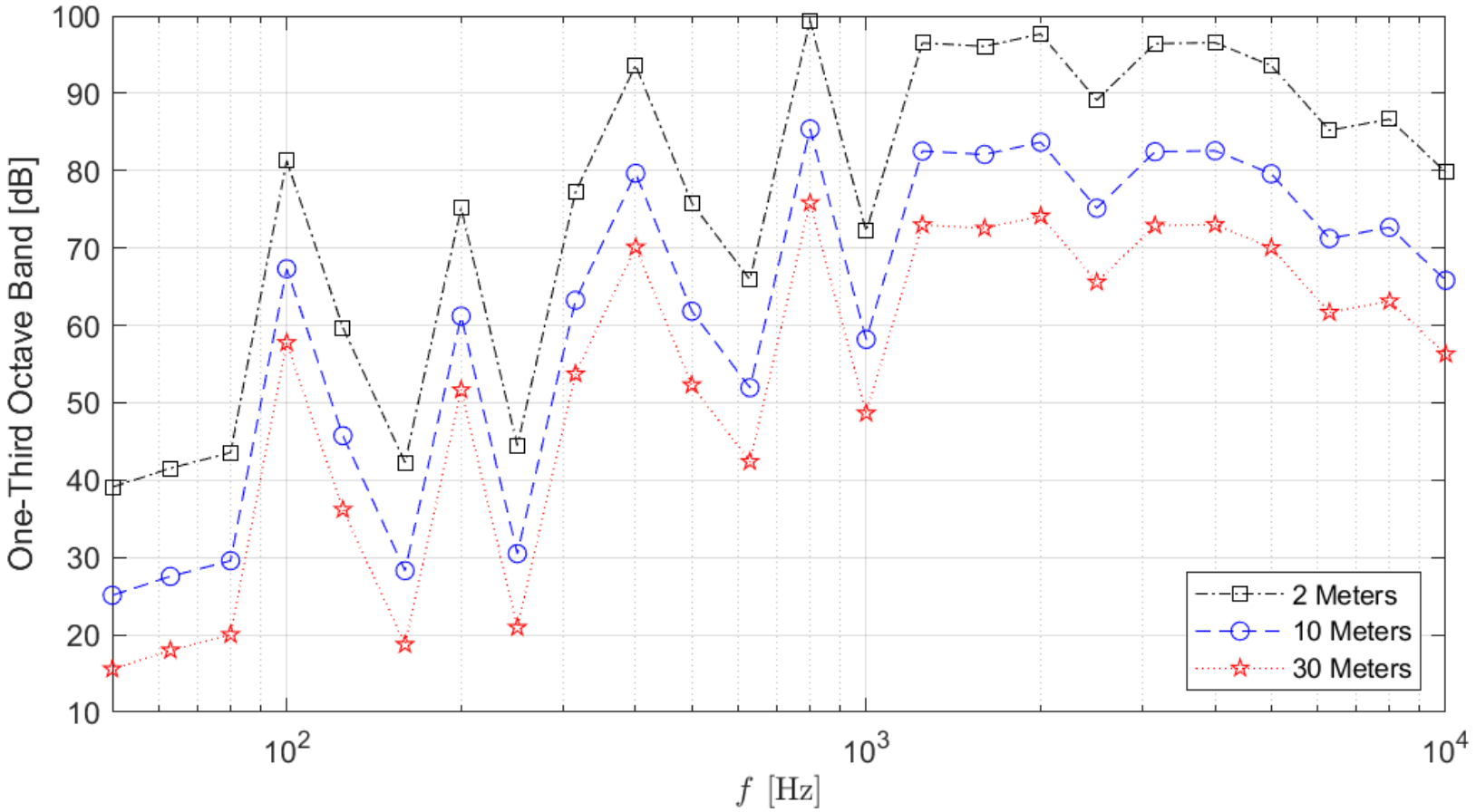

# MEASURED SOURCE NOISE IN MIL-STD-1474E FORM

| One-Third Octave Band Frequency (Hz) | Non-detectability Distance (meters) | | | | | | | | | | | | | | | | | | | |
|---|---|---|---|---|---|---|---|---|---|---|---|---|---|---|---|---|---|---|---|---|
| | 5 | 10 | 15 | 20 | 25 | 30 | 100 | 200 | 300 | 400 | 500 | 750 | 1,000 | 1,250 | 1,500 | 2,000 | 3,000 | 4,000 | 5,000 | 6,000 |
| 50 | 39 | 39 | 39 | 39 | 39 | 39 | 25 | 25 | 25 | 25 | 16 | 16 | 16 | 16 | 16 | 16 | 16 | 16 | 16 | 16 |
| 63 | 42 | 42 | 42 | 42 | 42 | 42 | 28 | 28 | 28 | 28 | 18 | 18 | 18 | 18 | 18 | 18 | 18 | 18 | 18 | 18 |
| 80 | 44 | 44 | 44 | 44 | 44 | 44 | 30 | 30 | 30 | 30 | 20 | 20 | 20 | 20 | 20 | 20 | 20 | 20 | 20 | 20 |
| 100 | 81 | 81 | 81 | 81 | 81 | 81 | 67 | 67 | 67 | 67 | 58 | 58 | 58 | 58 | 58 | 58 | 58 | 58 | 58 | 58 |
| 125 | 60 | 60 | 60 | 60 | 60 | 60 | 46 | 46 | 46 | 46 | 36 | 36 | 36 | 36 | 36 | 36 | 36 | 36 | 36 | 36 |
| 160 | 42 | 42 | 42 | 42 | 42 | 42 | 28 | 28 | 28 | 28 | 19 | 19 | 19 | 19 | 19 | 19 | 19 | 19 | 19 | 19 |
| 200 | 75 | 75 | 75 | 75 | 75 | 75 | 61 | 61 | 61 | 61 | 52 | 52 | 52 | 52 | 52 | | | | | |
| 250 | 44 | 44 | 44 | 44 | 44 | 44 | 30 | 30 | 30 | 30 | 21 | 21 | 21 | 21 | 21 | | | | | |
| 315 | 77 | 77 | 77 | 77 | 77 | 77 | 63 | 63 | 63 | 63 | 54 | 54 | 54 | 54 | 54 | | | | | |
| 400 | 94 | 94 | 94 | 94 | 94 | 94 | 80 | 80 | 80 | 80 | 70 | 70 | 70 | 70 | 70 | | | | | |
| 500 | 76 | 76 | 76 | 76 | 76 | 76 | 62 | 62 | 62 | 62 | 52 | 52 | 52 | 52 | 52 | | | | | |
| 630 | 66 | 66 | 66 | 66 | 66 | 66 | 52 | 52 | 52 | 52 | 42 | 42 | 42 | 42 | 42 | | | | | |
| 800 | 99 | 99 | 99 | 99 | 99 | 99 | 85 | 85 | 85 | 85 | 76 | 76 | 76 | 76 | 76 | | | | | |
| 1,000 | 72 | 72 | 72 | 72 | 72 | 72 | 58 | 58 | 58 | 58 | 49 | 49 | 49 | 49 | 49 | | | | | |
| 1,250 | 97 | 97 | 97 | 97 | 97 | 97 | 83 | 83 | 83 | 83 | 73 | 73 | 73 | 73 | 73 | | | | | |
| 1,600 | 96 | 96 | 96 | 96 | 96 | 96 | 82 | 82 | 82 | 82 | 73 | 73 | 73 | 73 | 73 | | | | | |
| 2,000 | 98 | 98 | 98 | 98 | 98 | 98 | 84 | 84 | 84 | 84 | 74 | 74 | 74 | 74 | 74 | | | | | |
| 2,500 | 89 | 89 | 89 | 89 | 89 | 89 | 75 | 75 | 75 | 75 | 66 | 66 | 66 | 66 | 66 | | | | | |
| 3,150 | 96 | 96 | 96 | 96 | 96 | 96 | 82 | 82 | 82 | 82 | 73 | 73 | 73 | 73 | 73 | | | | | |
| 4,000 | 97 | 97 | 97 | 97 | 97 | 97 | 83 | 83 | 83 | 83 | 73 | 73 | 73 | 73 | 73 | | | | | |
| 5,000 | 94 | 94 | 94 | 94 | 94 | 94 | 80 | 80 | 80 | 80 | 70 | 70 | 70 | 70 | 70 | | | | | |
| 6,300 | 85 | 85 | 85 | 85 | 85 | 85 | 71 | 71 | 71 | 71 | 62 | 62 | 62 | 62 | 62 | | | | | |
| 8,000 | 87 | 87 | 87 | 87 | 87 | 87 | 73 | 73 | 73 | 73 | 63 | 63 | 63 | 63 | 63 | | | | | |
| 10,000 | 80 | 80 | 80 | 80 | 80 | 80 | 66 | 66 | 66 | 66 | 56 | 56 | 56 | 56 | 56 | 56 | 56 | 56 | 56 | 56 |
| | 2 | 2 | 2 | 2 | 2 | 2 | 10 | 10 | 10 | 10 | 30 | 30 | 30 | 30 | 30 | 30 | 30 | 30 | 30 | 30 |
| | Measurement Distance (meters) | | | | | | | | | | | | | | | | | | | |

One-third octave band data repeated into the MIL-STD-1474E table

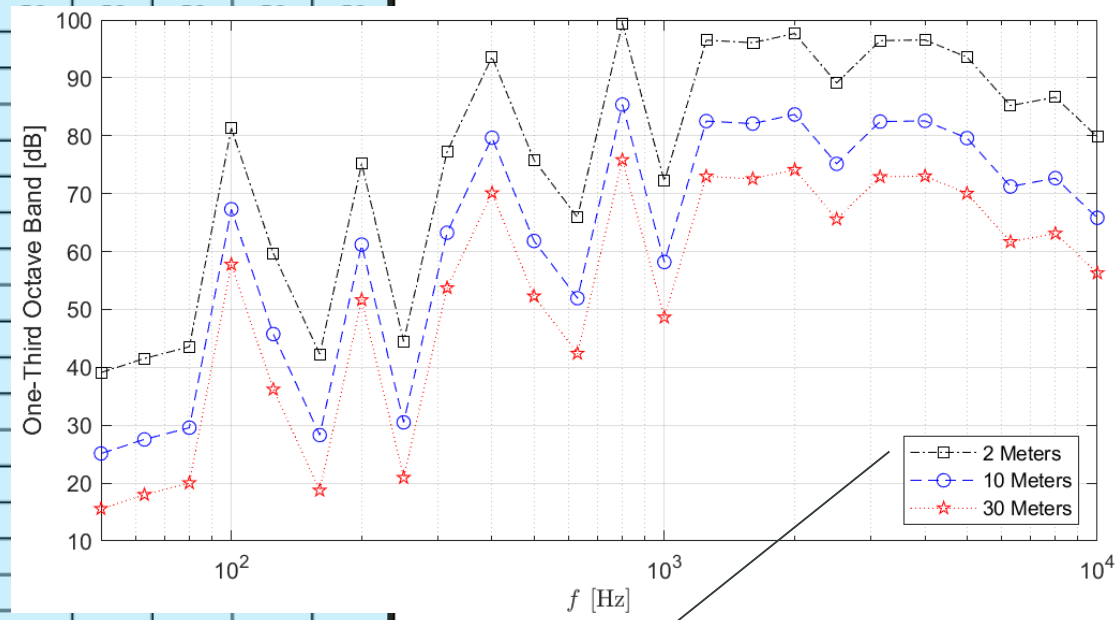

# DATA ANALYSIS

| One-Third Octave Band Frequency (Hz) | Non-detectability Distance (meters) | | | | | | | | | | | | | | | | | | | |
|---|---|---|---|---|---|---|---|---|---|---|---|---|---|---|---|---|---|---|---|---|
| | 5 | 10 | 15 | 20 | 25 | 30 | 100 | 200 | 300 | 400 | 500 | 750 | 1,000 | 1,250 | 1,500 | 2,000 | 3,000 | 4,000 | 5,000 | 6,000 |
| 50 | -9 | -14 | -17 | -20 | -22 | -23 | -37 | -43 | -46 | -49 | -50 | -54 | -57 | -59 | -60 | -63 | -68 | -71 | -74 | -76 |
| 63 | -2 | -8 | -11 | -14 | -16 | -17 | -31 | -37 | -41 | -43 | -46 | -50 | -53 | -55 | -57 | -60 | -65 | -69 | -73 | -76 |
| 80 | 0 | -5 | -9 | -11 | -13 | -14 | -30 | -36 | -39 | -42 | -45 | -49 | -52 | -55 | -57 | -61 | -67 | -73 | -77 | -81 |
| 100 | 40 | 35 | 31 | 29 | 27 | 25 | 8 | 2 | -2 | -5 | -7 | -12 | -15 | -19 | -21 | -26 | -34 | -41 | -46 | -49 |
| 125 | 23 | 19 | 15 | 13 | 11 | 9 | -12 | -18 | -23 | -26 | -29 | -35 | -40 | -44 | -47 | -53 | -62 | -66 | -69 | -70 |
| 160 | 6 | 3 | 0 | -2 | -4 | -6 | -27 | -35 | -40 | -44 | -47 | -54 | -60 | -65 | -70 | -74 | -78 | -80 | -82 | -83 |
| 200 | 34 | 33 | 30 | 28 | 26 | 24 | 9 | 0 | -6 | -11 | -16 | -26 | -30 | -33 | -35 | -37 | -40 | -42 | -44 | -46 |
| 250 | -3 | 0 | -3 | -5 | -7 | -9 | -20 | -31 | -39 | -46 | -50 | -55 | -58 | -59 | -61 | -62 | -65 | -68 | -70 | -72 |
| 315 | 33 | 31 | 30 | 27 | 25 | 23 | 13 | 0 | -8 | -12 | -14 | -17 | -19 | -20 | -21 | -23 | -27 | -29 | -32 | -34 |
| 400 | 65 | 51 | 51 | 49 | 46 | 44 | 29 | 18 | 14 | 12 | 8 | 6 | 4 | 3 | 1 | -1 | -5 | -8 | -11 | -14 |
| 500 | 50 | 34 | 29 | 27 | 25 | 22 | 8 | 0 | -2 | -4 | -3 | -6 | -8 | -9 | -11 | -13 | -18 | -21 | -25 | -28 |
| 630 | 39 | 29 | 21 | 17 | 14 | 12 | -3 | -11 | -15 | -16 | -11 | -14 | -16 | -18 | -19 | -22 | -27 | -32 | -36 | -40 |
| 800 | 69 | 68 | 62 | 58 | 55 | 52 | 31 | 22 | 19 | 17 | 22 | 19 | 17 | 15 | 13 | 10 | 4 | -1 | -6 | -11 |
| 1,000 | 47 | 43 | 39 | 35 | 32 | 30 | 8 | -1 | -5 | -7 | -5 | -8 | -11 | -13 | -15 | -19 | -25 | -31 | -37 | -42 |
| 1,250 | 74 | 66 | 65 | 63 | 60 | 58 | 41 | 31 | 26 | 24 | 19 | 16 | 13 | 11 | 8 | 4 | -3 | -10 | -17 | -23 |
| 1,600 | 74 | 65 | 64 | 64 | 63 | 61 | 46 | 36 | 31 | 28 | 21 | 17 | 14 | 11 | 9 | 4 | -5 | -14 | -22 | NAN |
| 2,000 | 77 | 73 | 63 | 66 | 67 | 66 | 48 | 37 | 32 | 29 | 24 | 20 | 16 | 12 | 9 | 3 | -8 | -19 | NAN | NAN |
| 2,500 | 71 | 63 | 63 | 53 | 57 | 58 | 47 | 36 | 30 | 27 | 20 | 14 | 10 | 6 | 2 | -6 | -20 | NAN | NAN | NAN |
| 3,150 | 80 | 75 | 72 | 69 | 60 | 62 | 53 | 42 | 36 | 32 | 32 | 26 | 20 | 14 | 9 | -1 | -21 | NAN | NAN | NAN |
| 4,000 | 82 | 76 | 72 | 72 | 70 | 63 | 58 | 46 | 39 | 34 | 33 | 24 | 16 | 9 | 1 | -13 | NAN | NAN | NAN | NAN |
| 5,000 | 82 | 76 | 72 | 67 | 70 | 69 | 57 | 45 | 37 | 30 | 22 | 10 | -1 | -12 | -22 | NAN | NAN | NAN | NAN | NAN |
| 6,300 | 70 | 65 | 62 | 60 | 54 | 55 | 44 | 31 | 21 | 13 | 6 | -11 | -27 | NAN | NAN | NAN | NAN | NAN | NAN | NAN |
| 8,000 | 64 | 57 | 54 | 52 | 50 | 48 | 33 | 19 | 6 | -5 | -16 | NAN | NAN | NAN | NAN | NAN | NAN | NAN | NAN | NAN |
| 10,000 | 55 | 49 | 45 | 43 | 41 | 38 | 19 | 2 | -15 | -30 | NAN | NAN | NAN | NAN | NAN | NAN | NAN | NAN | NAN | NAN |
| | 2 | 2 | 2 | 2 | 2 | 2 | 10 | 10 | 10 | 10 | 30 | 30 | 30 | 30 | 30 | 30 | 30 | 30 | 30 | 30 |
| | Measurement Distance (meters) | | | | | | | | | | | | | | | | | | | |

Red = detectable at that frequency and detection distance

Green = non-detectable at that frequency and distance

# UAS AURAL DETECTION

## CONDITION

$M_{TUN}$ = 0.111 (38 m/s)

RPM = 6000

Yaw = 0°

Background = Level 1

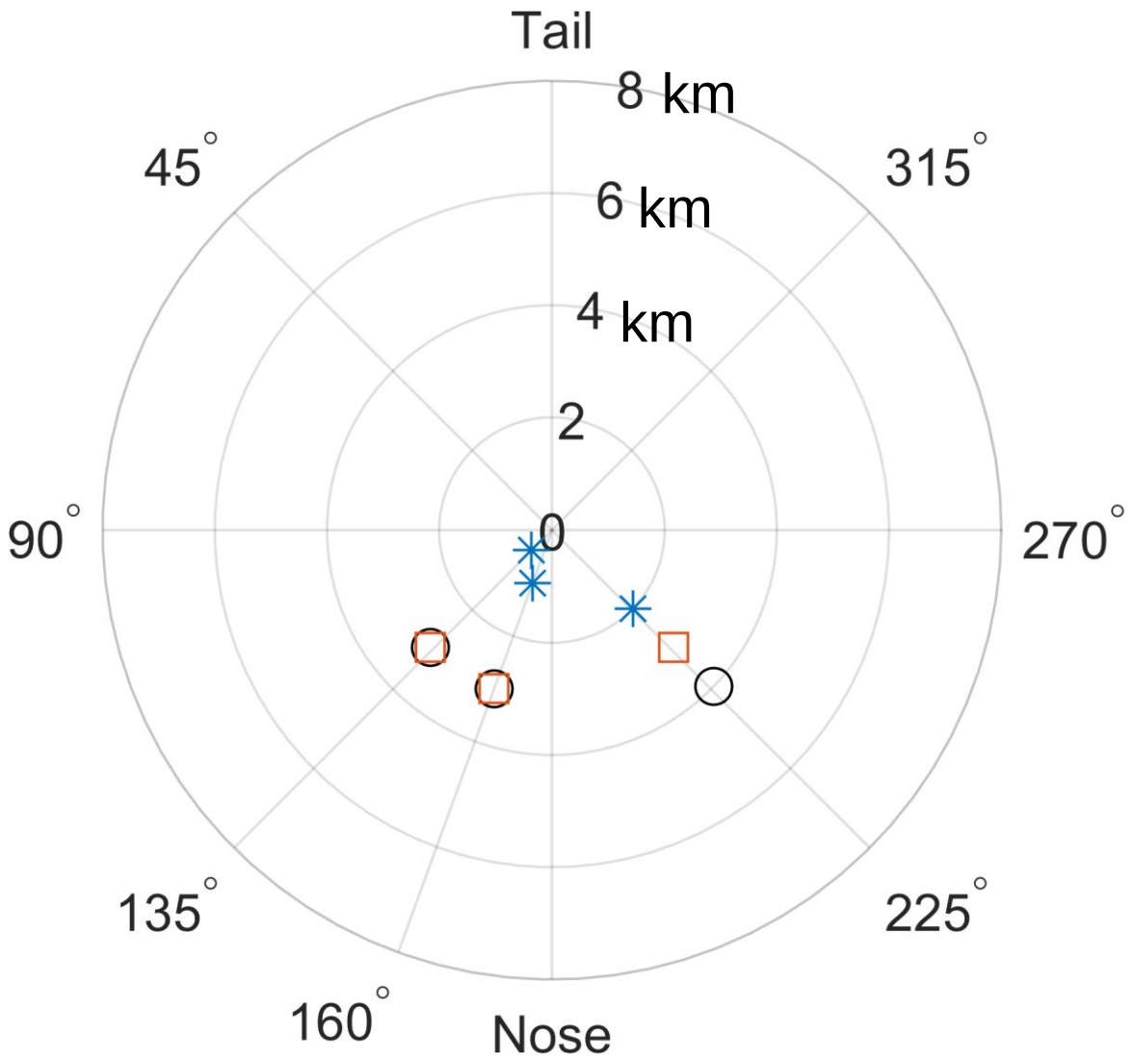


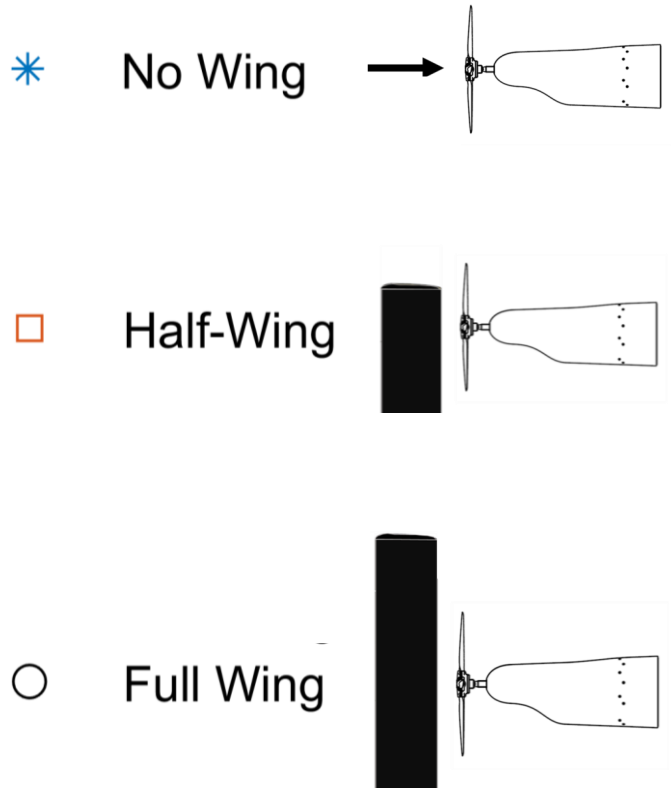

# UAS AURAL DETECTION

## CONDITION

$M_{TUN}$ = 0.111 (38 m/s)

RPM = 6500

Yaw = 0°

Background = Level 1

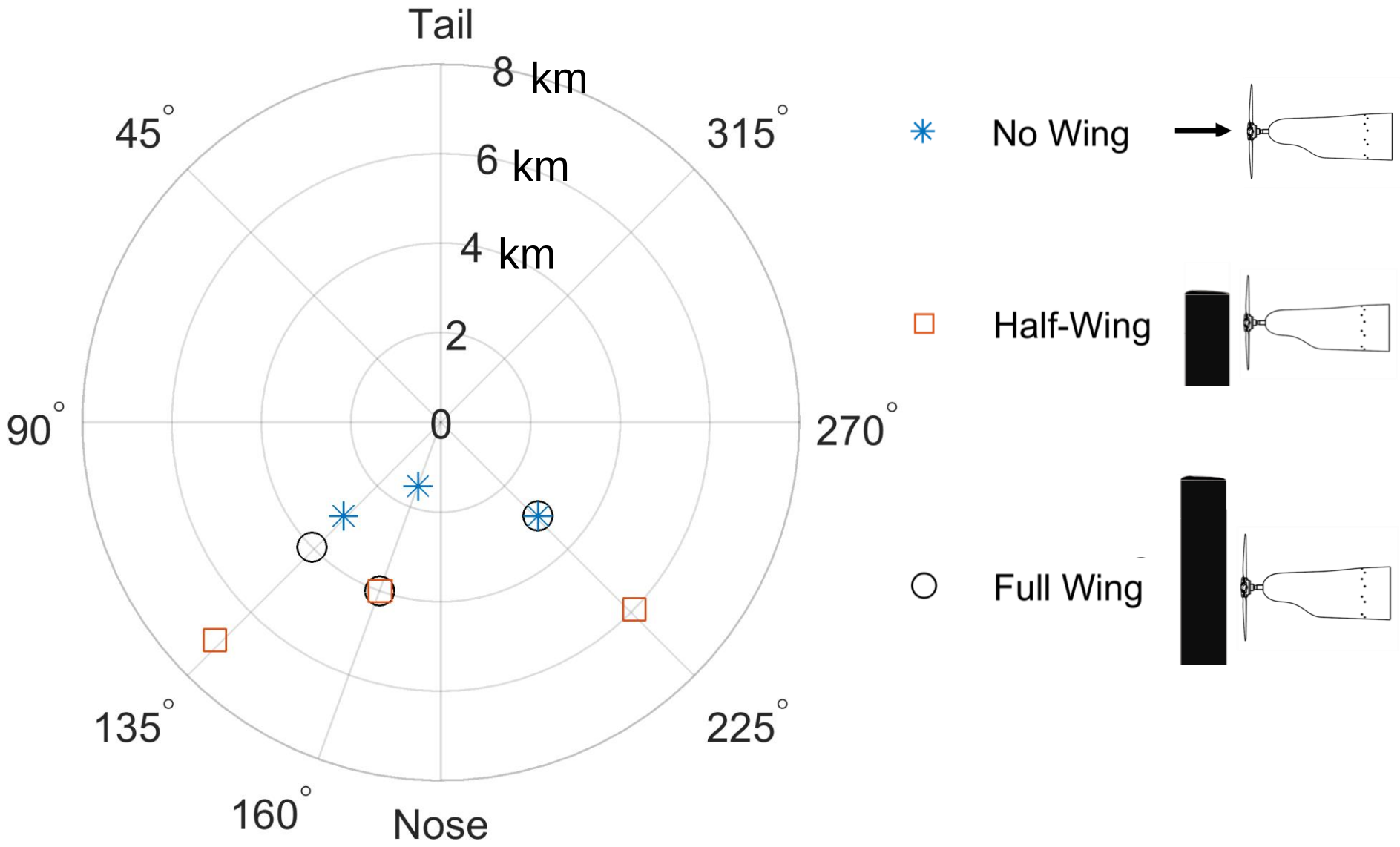

# WRAP-UP AND CONCLUSIONS

- **MIL-STD-1474E is capable of being used on wind tunnel data**
- **Up-stream bodies significantly impact acoustic emissions**
- **Acoustic impacts are tactically significant, according to MIL-STD-1473E analysis**

# QUESTIONS?

| | |
|---|---|
| **Website** | https://www.avmc.army.mil/ |
| **Facebook** | https://www.facebook.com/DEVCOM.AvMC |
| **Instagram** | https://www.instagram.com/DEVCOM_AvMC |
| **Twitter** | https://twitter.com/devcom_avmc |
| **LinkedIn** | https://www.linkedin.com/company/devcom-avmc |
| **Public Affairs** | usarmy.redstone.ccdc-avmc.mbx.pao@mail.mil |

# UAS AURAL DETECTION

## CONDITION

$M_{TUN}$ = 0.204 (70 m/s)

RPM = 6000

Yaw = 0°

Background = Level 1

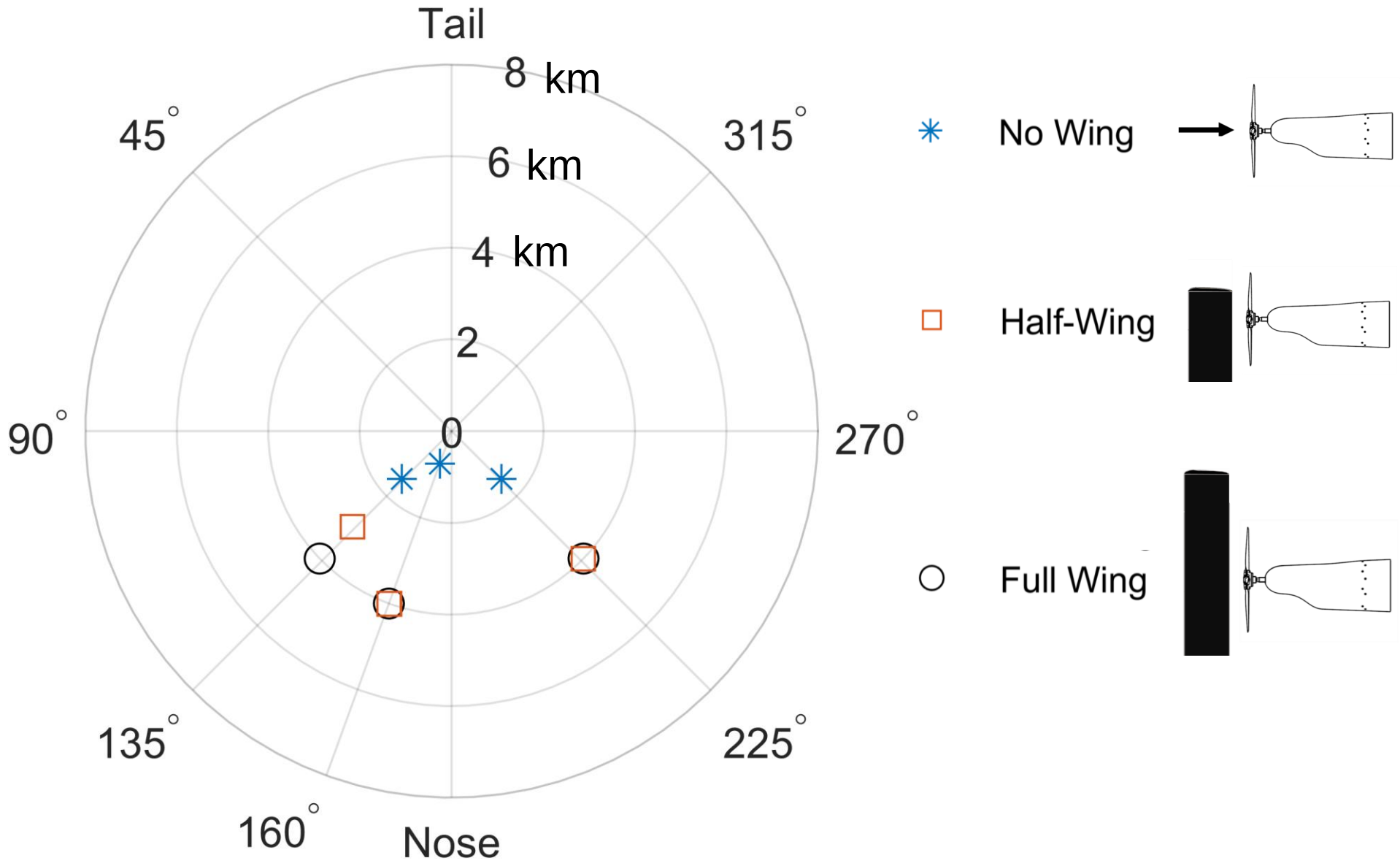

# UAS AURAL DETECTION

## CONDITION

$M_{TUN}$ = 0.204 (70 m/s)

RPM = 6500

Yaw = 0°

Background = Level 1

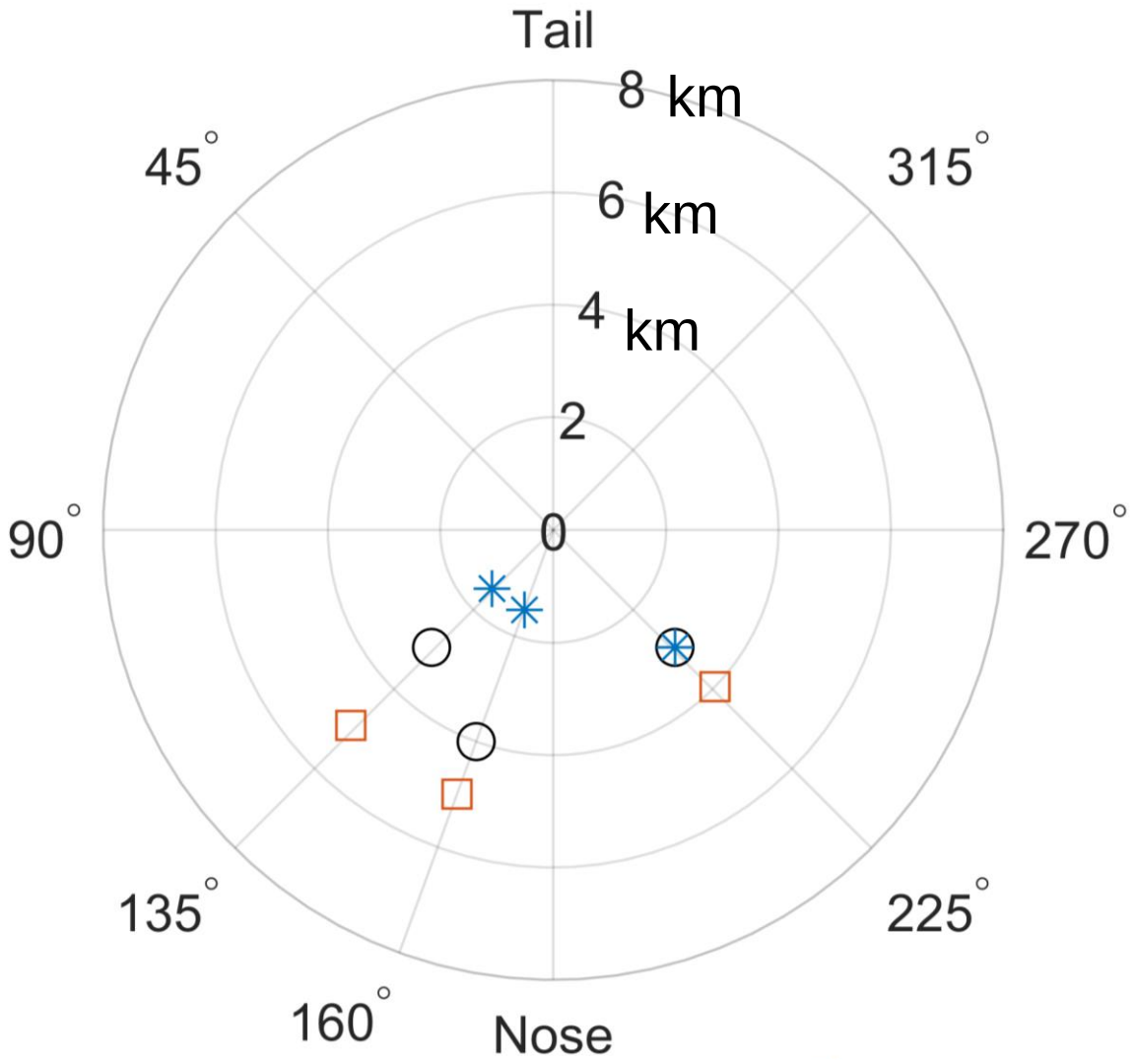


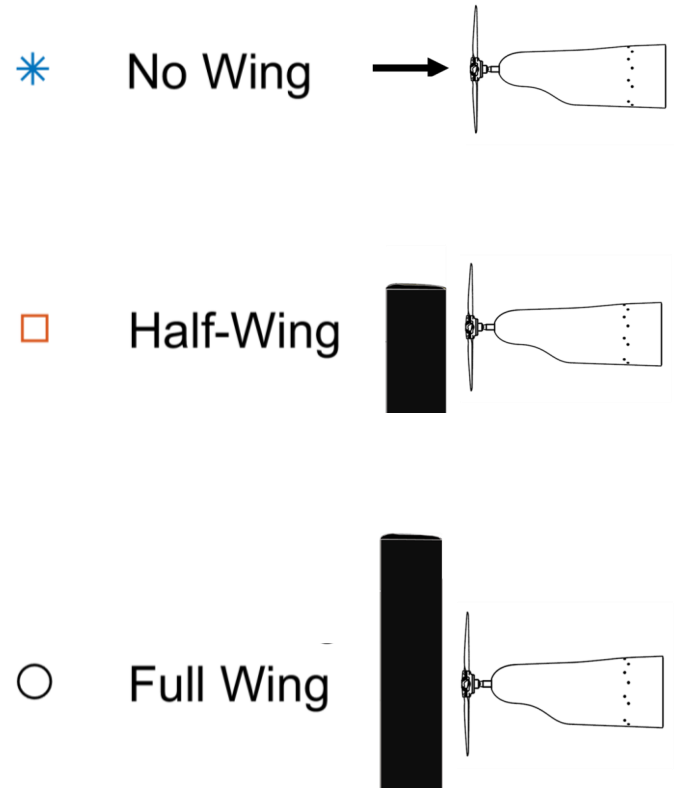

# UAS AURAL DETECTION

## CONDITION

$M_{TUN}$ = 0.111 (38 m/s)

RPM = 6000

Yaw = 0°

Background = Level 2